IOP Publishing Journal of Physics D: Applied Physics
J. Phys. D: Appl. Phys. **56** (2023) 353001 (20pp) https://doi.org/10.1088/1361-6463/acd2e5

Topical Review

A review on recent progress in organic photovoltaic devices for indoor applications

Gautham Kumar[1] **and Fang-Chung Chen**[1,2,*]

[1] Department of Photonics, College of Electrical and Computer Engineering, National Yang Ming Chiao Tung University, Hsinchu 30010, Taiwan
[2] Center for Emergent Functional Matter Science, National Yang Ming Chiao Tung University, Hsinchu 30010, Taiwan

E-mail: fcchen@mail.nctu.edu.tw and fcchendop@nycu.edu.tw

Received 1 February 2023, revised 6 April 2023
Accepted for publication 5 May 2023
Published 1 June 2023

Abstract

Organic photovoltaics (OPVs) have shown great potential as a new generation of energy sources because they possess many unique properties, including mechanical flexibility, light weight, semitransparency, and low fabrication costs. In particular, OPV devices exhibit high power conversion efficiencies under indoor and low-level lighting conditions. Therefore, they can function as promising energy sources in low-light or cloudy environments for many applications, including the Internet of Things, wearable electronics, and sensors. In this article, we review recent progress in OPV devices for these special applications. We start with an introduction to the fundamental principles of OPVs. Then, we review the preparation and design principles of the photoactive layers for indoor applications. We also highlight the importance of interlayers in high-performance photovoltaic devices under indoor and/or low-level lighting illumination conditions. Recent efforts to improve the efficiencies of indoor OPV devices using plasmonic nanostructures are also summarized. Finally, we examine the progress in large-area devices and modules for indoor and/or low-level lighting applications. We believe that the rapid progress in indoor OPV cells and modules will trigger the development of low-cost, highly efficient OPV products for indoor applications in the near future.

Keywords: polymer, organic, photovoltaics, indoor, solar cell, solar module, plasmonic nanostructures

(Some figures may appear in color only in the online journal)

1. Introduction

Organic photovoltaics (OPVs) have shown great potential as a new generation of energy sources because of their unique properties, including mechanical flexibility, light weight, semitransparency, and low fabrication cost [1–3]. Benefiting from in-depth research on device physics [4] and advancements in organic materials [4–8], OPV devices have made significant advances in device performance. The most efficient OPV cells have achieved outstanding power conversion efficiencies (PCEs) of more than 18% under standard solar irradiation conditions (100 mW cm^{-2}, AM 1.5G) [9]. Nonetheless, OPV cells are still grappling with numerous

* Author to whom any correspondence should be addressed.

Figure 1. Smart device applications acquire low power energy from photovoltaics under ambient light conditions.

difficulties when it comes to utilizing them for outdoor solar applications. For example, OPV devices are still highly susceptible to moisture and high air temperatures, and organic materials degrade easily under such extreme working conditions. Moreover, the large-scale manufacture of large-area solar modules has yet to achieve maturity.

The emergence of the Internet of Things (IoTs) has resulted in an unprecedented surge in the number of indoor appliances in various aspects of our daily life [10, 11]. IoT systems interact wirelessly among a massive amount of electronics and sensors with unique identifiers and real-time data, and digital information can be collected by or exchanged among the nodes, devices, and actuators [12–15]. Nevertheless, these off-grid devices require extensive energy sources to maintain the functionality of IoT systems [16]. In order to enhance their sustainability, renewable energy technologies are particularly critical. Among the renewable energy sources that can generate power conveniently from the surrounding environment, photovoltaic technology in particular can provide high voltages and high energy densities. OPV technology has been reported to achieve PCE values of approximately 30% when exposed to indoor lighting conditions [17–22]. Recent research indicates that this technology is capable of harnessing energy from indoor lighting and generating microwatt to milliwatt power, which is adequate to operate and/or assist with the charge of many electronic devices [16]. For instance, applications include smart homes, the IoT, wearable electronics, sensors, and industrial automation (figure 1) [16, 23]. Therefore, OPV cells are highly desirable for indoor applications [24].

There are several types of OPV devices: polymer solar cells (PSCs), small molecular solar cells (SMSCs), and dye-sensitized solar cells (DSSCs) [23]. The structure of PSCs typically consists of a blend of a polymer donor and a small molecular acceptor that creates a bulk heterojunction (BHJ). SMSCs are made of small organic molecules and have a similar working principle to PSCs. They are often fabricated using vacuum evaporation methods, which are usually considered costly processes. Therefore, they are typically more difficult and expensive to manufacture. Meanwhile, DSSCs usually use dye molecules to absorb light and generate electrical energy. The basic structure of a DSSC consists of a transparent conducting electrode (TCE), an inorganic semiconductor layer, such as TiO_2 coated with dyes, an electrolyte solution, and a counter electrode. DSSCs are relatively inexpensive and easy to manufacture. They also work very well under low-light conditions, making them suitable for use in indoor environments [23]. In this review, we focus on OPV cells that are prepared using conventional wet processes.

Indoor photovoltaics (IPVs) have the potential to solve these hardware issues for future IoT ecosystems, providing greater reliability and longer operational lifetimes for various applications. Persistent powering of individual appliances by harvesting ambient light using small $\sim cm^2$ photovoltaic cells is becoming possible for more and more wireless technologies and devices [25, 26]. Unfortunately, investigation still lags behind the increasing need for electrical power. To further improve the performance of OPV cells for indoor applications, a deeper comprehension of device physics is needed. Finally, despite the rapid advancements in device and materials research, new characterization difficulties, including diverged beams and inhomogeneous light distribution have made device performance reports less reliable than those prepared under conventional air mass 1.5 global (AM) 1.5G illumination conditions.

Currently, reviews focused on recent advancements in indoor OPV applications are still rare compared to those for outdoor OPV applications. In this review article, we first discuss briefly the underlying working mechanisms of OPV cells, and provide insights into the requirements of photoactive and interfacial layers under indoor conditions. We then review and summarize recent progress in the development of OPV cells for indoor applications. Finally, conclusions are made, and an outlook for future challenges is also discussed.

2. Device physics of OPV devices

To enhance the performance of OPV devices, it is essential to have a comprehensive understanding of the physical mechanisms that occur within the cells. Figure 2 illustrates the fundamental physical processes responsible for generating the photocurrent upon solar irradiation. Incident photons are absorbed by the organic semiconductors (1), creating bounded excitons. These excitons diffuse (3) throughout the organic materials (donor molecule in figure 2(a)). When they encounter an interface between the organic donor and acceptor molecules, the strong binding energy of the excitons can be overcome. Therefore, the excitons are quickly dissociated (4) to produce separated charges [27, 28]. The separated free electrons

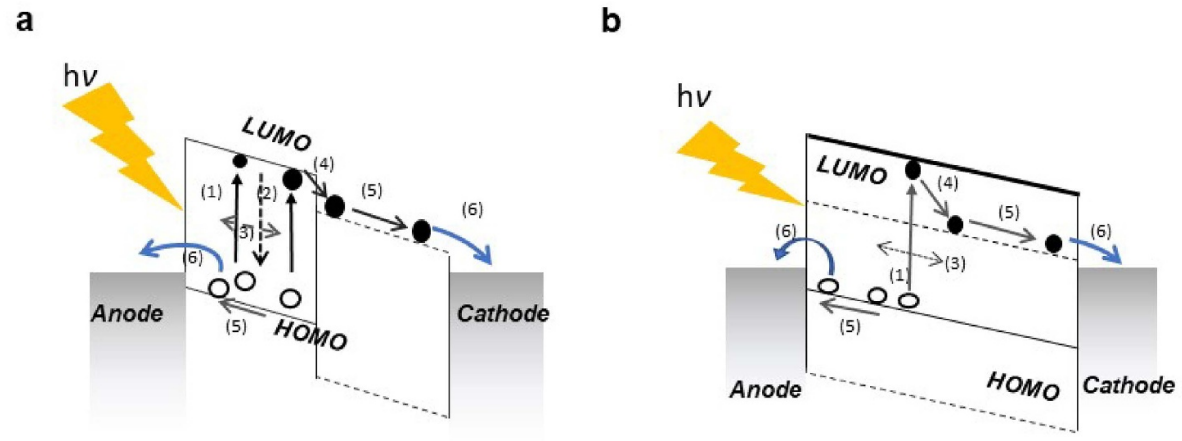

Figure 2. Schematic illustration of (a) a bilayer device and (b) a bulk heterojunction device. Numbers indicate the physical processes described in the text.

and holes transport (5) to their corresponding electrodes (6) within their respective lifetimes, and the photocurrent is generated after they are collected by the electrodes. However, some excitons may decay (2) and produce luminance when they are far from the donor/acceptor interfaces. Therefore, it is crucial for excitons to be formed within their diffusion length close to the interface.

During step (1) of the above photovoltaic processes, the active layers capture a fraction of the incident light. For example, a semiconductor with a bandgap of 1.1 eV is able to absorb more than 70% of the solar irradiation. Therefore, it is very critical to have an optimized bandgap to harvest most of the photons. Organic semiconductors usually possess high absorption coefficients and this property somehow compensates for the low mobility of organic semiconductors. The typical thickness of a photoactive layer is around a hundred nanometers, which is close to the absorption length of the organic materials in the OPV cells. A photoactive layer that is too thick will lead to a low charge collection efficiency. Furthermore, the dielectric constants of organic materials are relatively lower than those of inorganic semiconductors; the low dielectric constants result in strongly bound Frenkel excitons. Therefore, unlike the free charges created in Si solar cells, the exciton binding energy is strong at room temperature in organic materials. In other words, the thermal energy at room temperature is insufficient to split photogenerated excitons into free charge carriers. As a result, the configuration and working principles of OPV devices differ greatly from those made of inorganic semiconductors. The exciton diffusion length (L_D), which describes the effective length that an exciton can diffuse, has been found to be 5–8 nm for organic semiconductors [29–31]. The efficiency of a bilayer cell (figure 2(a)) is constrained by the number of photons that can be absorbed within the range equal to the L_D at the donor–acceptor interface because the photon absorption length is often larger than the L_D value in organic films.

At the interfaces between materials with sufficiently dissimilar electron affinities and ionization potentials, the exciton binding energy can be overcome and photogenerated excitons can be split into free charges. In other words, if the offset energy difference between the lowest unoccupied molecular orbitals (LUMOs) for the donor and acceptor is larger than the exciton binding energy, exciton dissociation could take place at the donor–acceptor interface (4). On the other hand, if the energy difference is not sufficient, the excitons may eventually recombine, resulting in energy loss. The free electrons and holes move to the cathode and anode, respectively, after the excitons separate. Many different mechanisms, including the gradient in the chemical potentials of the electrons and holes at the donor–acceptor interfaces, may drive the flow of the charge carrier [32]. The charge transport could also be affected by recombination between the charges [33].

In most cases, OPV devices with a BHJ structure (figure 2(b)) exhibit higher efficiencies than devices prepared with a bilayer structure (figure 2(a)). The very limited contact area of the donor–acceptor interface in devices prepared using a bilayer structure usually leads to a low photocurrent. For an OPV device prepared using the BHJ concept, the high interfacial area of the donor–acceptor interfaces ensures that the carrier generation efficiency can be approximately close to 100%. On the other hand, the charge collection efficiency is significantly affected by the relative arrangement of the donor and acceptor materials. Such morphology of the photoactive layer is often the most critical factor affecting device PCEs. The morphology of the photoactive layers is mainly determined by the physical properties of the materials, such as their crystallinity, solubility, and/or miscibility [34–36].

The divided charges must go through the photoactive layer–electrode interfaces in order to reach the external circuit (6). The nature of the interface between the photoactive layer and the electrodes affects the charge collection efficiency significantly. Charge extraction, which is a complicated process, strongly depends on the chemical nature of the organic semiconductor–electrode interface (e.g. Al, Ca) and the morphology of the photoactive layers. Many factors, including the diffusion of ions or metal atoms into the organic layer [37], chemical reactions [38], interfacial dipoles at the contacts, and band bending [39], can affect the energetics at the interface and influence the extraction process.

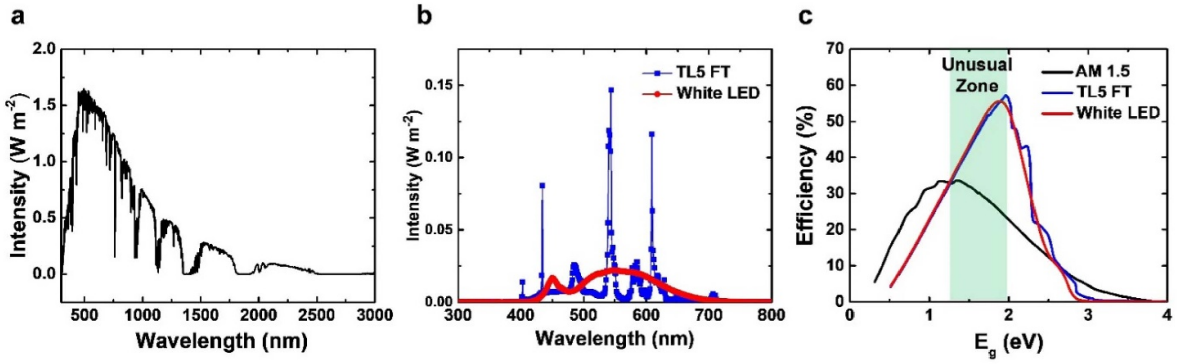

Figure 3. (a) Standard solar spectrum [49]; (b) the spectra of a fluorescent tube (FT) and a white LED; (c) the calculated maximum power conversion efficiencies versus material bandgaps under either an FT, a white LED, or solar irradiation. The ideal bandgap energy is near 1.9 eV for indoor conditions [47]. John Wiley & Sons. © 2019 WILEY-VCH Verlag GmbH & Co. KGaA, Weinheim.

3. Indoor light sources

Understanding the fundamental characteristics of indoor or low-power light sources is essential for designing high-performance indoor OPV devices. Two major differences, power intensity and spectral range, exist between sunlight and indoor lighting sources [40]. Compared with the standard solar spectrum (figure 3(a)), the typical emission spectra of indoor light sources, such as inorganic light-emitting diodes (LEDs) and fluorescent tubes (FTs), are usually narrow and range between 400 and 700 nm (figure 3(b)) [41–43]. With reducing prices, LEDs are expected to become the mainstream for indoor light sources in the near future. The spectra of frequently used indoor light sources are illustrated in figure 3(b). Moreover, the light power under indoor lighting conditions is usually less than 1 mW cm^{-2}, which is several orders lower than that of standard solar irradiation (AM 1.5G; 100 mW cm^{-2}). The light intensity in normal offices or shopping complexes is three orders of magnitude lower and most light illuminance conditions are well within the range from 200 lux to 1000 lux [44]. Note that the units of light intensity for the two types of light sources are also very different. While solar irradiation is usually measured in terms of energy (power), the intensity of indoor light sources is more often defined using a photometric quantity, called luminous flux (Φ), which is in units of lumens (lm). For many applications, photometry is more concerned with the amount of light falling on a unit area of a surface and such a light quantity is called the 'illuminance' (E). The unit of illuminance is commonly lm m^{-2} or lux. Additionally, photometry considers visible light due to its correlation to the visual sensation. More details on the background of the units for indoor lighting can be found in [23]. The above two major differences lead to entirely different design rules for efficient IPVs, and a single device can also perform very differently under two different illumination conditions. For example, the carrier density is much lower in OPV cells for indoor applications [14, 16].

As a result of less photogenerated charges, OPVs produce a lower current density (J_{sc}). However, the fill factor (FF) can be increased because of the lower level of charge recombination [45], possibly leading to a higher PCE value. Additionally, the reduced incident light intensity has an impact on the open-circuit voltage (V_{oc}) [25]. In a traditional diode model, it approximately decreases as a function of the logarithm of the device photocurrent,

$$V_{OC} \approx \frac{nkT}{e} \ln \frac{I_{ph}}{I_{dark}}, \quad (1)$$

where n is the ideality factor, k is the Boltzmann constant, T is the temperature, e is the elementary charge, I_{dark} is the dark current, and I_{ph} is the photocurrent. It can be deduced from equation (1) that higher V_{oc} values could be obtained when the dark current is low; i.e. high bandgap semiconductors [46]. In other words, devices with higher shunt resistances may exhibit higher PCEs due to improved V_{oc} values.

Different to sunlight irradiation, which has a wide spectral regime from the ultraviolet–visible (UV–vis) to the infrared (IR) range, the optimized bandgaps for IPVs are preferred to be wider according to the calculation results from the Shockley–Queisser model [47]. Freunek and Reindl proposed that a bandgap between 1.9 and 2.0 eV is most appropriate for indoor light harvesting [48]. As shown in figure 3(c), the optimum bandgap for low-power systems (LEDs and FTs) is close to 1.9 eV, rather than that of ∼1.4 eV for standard sunlight [48]. The calculation results also reveal that a narrow absorption band smaller than 700 nm can decrease the power output, resulting in lower open-circuit voltage (V_{oc}) values, under either white LEDs or FTs. Furthermore, an unusual zone is found in which the dependence of the PCEs on the bandgap under illumination from indoor lighting sources follows trends different from that under solar irradiation. In other words, photovoltaic devices for indoor applications exhibiting high performance under solar irradiation may not perform well under indoor lighting conditions [48].

4. Polymer photovoltaics for indoor applications

4.1. Active layers

This review mainly focuses on systems of photoactive layers that consist of conjugated polymers as the donor and fullerene,

Table 1. Fullerene-based photovoltaic (PV) device performance under indoor light conditions.

Active layer	Light source/illumination (lux)	V_{oc} (V)	J_{sc} (mA cm^{-2})	*FF* (%)	PCE (%)	Pout (μW cm^{-2})	References
P3HT:$PC_{61}BM$	FL/1000	—	—	—	7	19	[52]
PTB7-Th:$PC_{71}BM$	LED/890	0.62	0.092	74	11.63	42.3	[53]
PCE-10:$PC_{71}BM$	LED (20.5 mW.cm^{-2})	—	—	—	21.04	—	[14]
PCDTBT:$PC_{71}BM$	FL/300	0.41	0.0277	69.3	16.6	17.08	[25]
P3HT:$PC_{61}BM$	FL/500	0.43	0.062	59	9.59	15.77	[40]
P3HT:ICBA	FL/500	0.73	0.050	62	13.76	22.57	[40]
PTB7-Th:$PC_{71}BM$	FL/500	0.58	0.063	59	13.14	21.56	[40]
PCE-10:$PC_{71}BM$	FL/1000	0.63	0.119	59	13.42	44	[54]
PCE-10:$PC_{71}BM$	LED/1000	0.65	0.117	57	12.28	43	[54]
BTR:$PC_{71}BM$	FL/1000	0.791	0.133	75.2	28.1	78.2	[51]
PCDTBT:$PC_{71}BM$	LED/300	0.737	0.0311	63.4	18.72	14.53	[55]
P1:$PC_{71}BM$	LED (3000 K)/300	0.758	0.02956	66.1	19.15	14.86	[55]
PTB7:$PC_{71}BM$	LED/500	0.60	0.046	54.3	9.11	15.487	[56]
P3HT:$PC_{71}BM$	LED/1000	0.498	0.0737	71.9	9.4	26.32	[17]
PBDB-T:$PC_{71}BM$	LED/1000	0.669	0.0902	71.3	15.3	42.84	[17]
$PDTBTB_Z$-$2F_{anti}$: $PC_{71}BM$	LED/1000	0.817	0.1124	70.4	23.1	64.68	[17]
PM6:$PC_{71}BM$	LED/1000	0.784	0.0941	67.1	18.1	54.69	[41]
WF_3:$PC_{71}BM$	LED/500	0.58	0.06	65.5	12.83	21.811	[57]
WF_3S:$PC_{71}BM$	LED/500	0.63	0.062	66.9	14.32	24.344	[57]
WF_3F:$PC_{71}BM$	LED/500	0.70	0.065	69	17.34	29.478	[57]
PPDT2FBT:$PC_{71}BM$	LED/1000	0.587	0.117	65.2	16	44.8	[58]
PPDT2FBT:$PC_{61}BM$	LED/1000	0.62	0.085	69.5	11.8	36.7	[59]
BDT-1T-ID:PNP	LED/200	0.84	0.0192	59	12.40	9.5	[60]
BDT-2T-ID:PNP	LED (2900 K)/200	0.75	0.0246	69	16.2	12.4	[60]
PTB7:PNP	LED/200	0.58	0.0193	68	9.9	7.6	[60]
1DTP-ID:PNP	LED/200	0.67	0.0246	68	19.3	11.2	[61]
2DTP-ID:PNP	LED/200	0.72	0.0228	63	17.8	10.3	[61]
PV2001:$PC_{61}BM$	FL/1000	4.81	0.104	60	13.4	37.734	[62]
PV2001:$PC_{61}BM$	LED/1000	4.89	0.124	61	13.0	46.199	[62]

or nonfullerene (NF) derivatives, as the acceptor. Where possible, the methodology of fabrication of the active layer is mentioned along with reported device efficiencies. The morphology of the photoactive layers is heavily affected by the processing steps, solvents, annealing methods, and annealing temperatures, and the resulting nanostructure plays a major role in determining the photovoltaic properties [35, 36, 50]. Furthermore, the donor–acceptor materials of the active layer should match absorption spectra with the indoor light spectrum (figure 3(b)). Therefore, using low bandgap materials to harvest as many photons as possible for the standard 1 sun illumination is probably not suitable for indoor systems. In the following sections, we discuss the indoor performance of devices prepared with various active layers.

4.1.1. Fullerene-based material systems. In the last few years, wide bandgap fullerene acceptors such as N-phenyl-2-phenyl[60]fulleropyrrolidine (PNP), indene-C_{60} bisadduct (ICBA), [6,6]-phenyl-C_{71}-butyric acid methyl ester ($PC_{71}BM$), and phenyl-C_{61}-butyric acid methyl ester ($PC_{61}BM$) have been blended with conjugated polymers to prepare indoor OPV devices (table 1 and figure 4(a)). PCE values ranging from 13% to 28% under illumination of indoor light sources have been reported [51]. In 2017, our group investigated the effects of energy levels on indoor performance using various combinations of model materials (figure 4(a)); a device prepared with regioregular poly(3-hexylthiophene) (P3HT) and ICBA achieved the best PCEs of 13.76% and 13.05% under 500 lux-illuminance of an FT and inorganic LEDs, respectively [40]. Devices prepared with P3HT:$PC_{61}BM$ and Poly{4,8-bis[5-(2-ethylhexyl)thiophen-2-yl]benzo[1,2-b:4,5-b']-dithiophene-2,6-diyl-alt-3-fluoro-2-[(2-ethylhexyl)carbonyl]-thieno[3,4-b]thiophene-4,6-diyl}, (PTB7-Th or PBDTTF-EFT): $PC_{71}BM$ blends exhibited lower PCEs because the lower energy offsets between the highest occupied molecular orbital (HOMO) of the polymer donor and the LUMO of the fullerene acceptors resulted in a lower V_{oc} (figure 4(b)). Hence, the performance of a device can be maximized through increasing the energy offset. Furthermore, because most materials systems could cover the visible spectral regime, the photocurrents would not be too different among various devices. Therefore, the photovoltage is presumably rather more critical for determining the overall performance of indoor OPV devices [40].

In 2018, the influence of solvent vapor annealing (SVA) on the active layer of fullerene-based OPV devices was reported by Lee *et al* [51]. A promising OPV material system has emerged using a blend of a small molecule donor and a fullerene acceptor, namely benzodithiophene terthiophene rhodamine:[6,6]-phenyl-C_{71}-butyric acid methyl ester (BTR:$PC_{71}BM$) [51]. The devices prepared with SVA

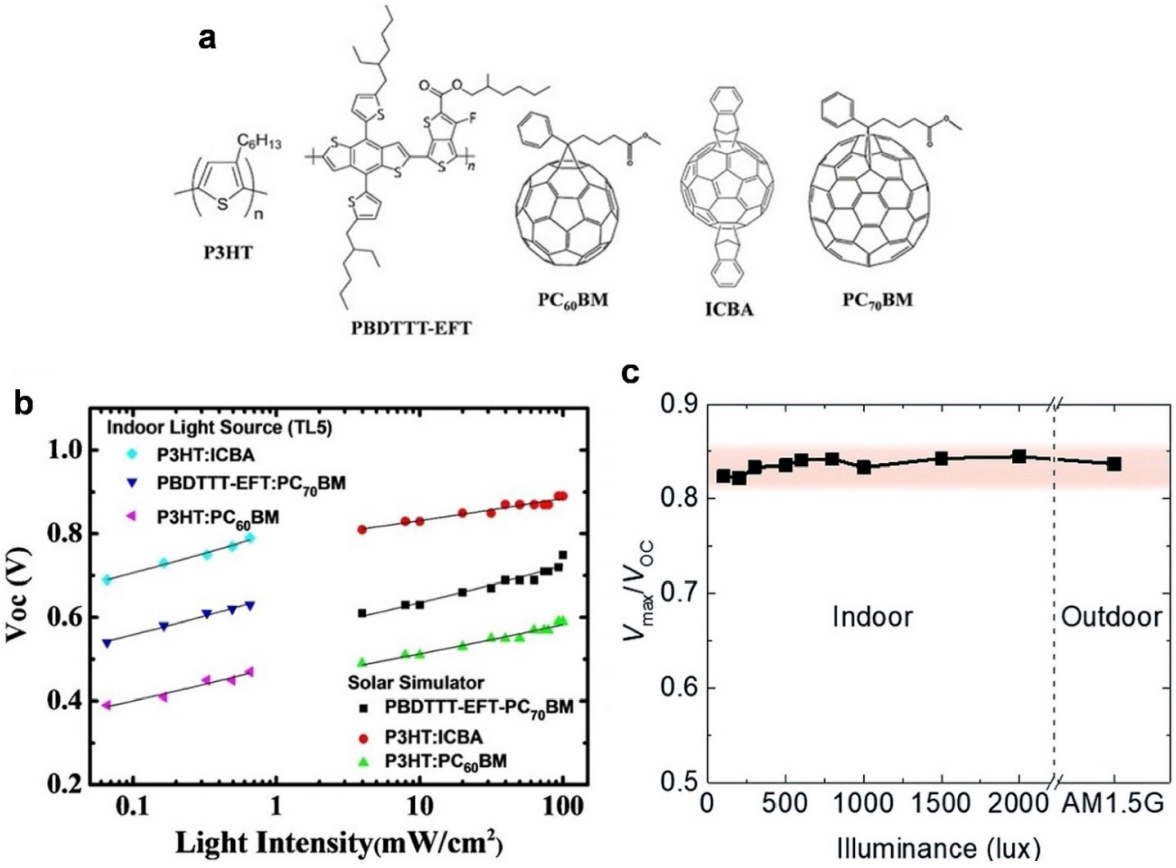

Figure 4. (a) Chemical structures of materials for indoor OPV cells, and (b) V_{oc} of the OPV devices under the intensity of the incident light. The lines are the corresponding fitting curves. [40] John Wiley & Sons. © 2017 WILEY-VCH Verlag GmbH & Co. KGaA, Weinheim. (c) V_{max}/V_{oc} ratio of a BTR:$PC_{71}BM$ device under indoor lighting and AM 1.5G conditions. Reproduced from [51] with permission from the Royal Society of Chemistry.

achieved a record PCE of 28.1% under irradiation of a fluorescent lamp at 1000 lux. The optimized SVA time could achieve appropriate growth of crystallization in the film morphology and balanced phase separation. The authors also defined a voltage fraction, which is the ratio of the V_{max} to the V_{oc}. The fraction could vary greatly under different light conditions because this ratio is closely related to the *FF*, which changes substantially with light intensity. However, the authors found that the voltage fraction was stable from 100 lux to 2000 lux and even up to 1 sun (AM 1.5G) illumination; the stable fraction could be attributed to the high and stable *FF* throughout the broad range of light levels (figure 4(c)). The ratio is important because the conventional maximum power point (MPP) tracking method used for outdoors may not be suitable for indoor applications. Instead, the fractional-voltage method, which employs a pre-set voltage fraction in a circuit to track the MPP, was perhaps more appropriate; this approach, in principle, consumes much less power compared to the MPP tracking method [63]. Stable ratios of $V_{max}/V_{oc,}$ which were proved in this work, clearly suggest that the fractional-voltage method is very suitable for small-power applications under low-level illumination conditions.

Meanwhile, Yin *et al* adopted comparative studies of the performance of two different donors (P1 and PCDTBT) with fullerene acceptors ($PC_{71}BM$) under indoor light conditions [55]. P1 is a donor designed following the concept of a symmetrical acceptor–donor–acceptor (A–D–A) structure and comprises a porphyrin ring with an aliphatic side-chain as a periphery substituent and connecting 3-ethylrhodanine units as the end groups (via phenylene ethylene bridges) [64]. Porphyrin donors have many advantages. They exhibit broad and high absorptivity from the visible to near-IR (NIR) regions and also possess a lower-lying HOMO energy level, allowing a high photovoltage of about 0.9 V with low energy losses [64]. Moreover, the use of long meso-alkyl chains facilitates π-stacking in the solid state, and their large planar π-conjugation macrocycles provide high carrier mobility and efficient intermolecular charge transfer, leading to high device *FF* and high solubility [65]. Lower V_{oc} loss and higher PCEs have been achieved under indoor conditions for the P1:$PC_{71}BM$ device; a PCE of 19.15% was reported under illumination of a 300 lux LED source (color temperature: 3000 K); the V_{oc} was 0.896 V under 1 sun illumination (AM 1.5G) and decreased to 0.758 V under illumination of an LED (300 lux). Additionally, the PCDTBT:$PC_{71}BM$ device exhibited a PCE of 18.72%; the V_{oc} value decreased from 0.923 V (1 sun, AM 1.5G) to 0.737 V under illumination from an LED (300 lux). Moreover, compared with PCDTBT, the porphyrin donor P1

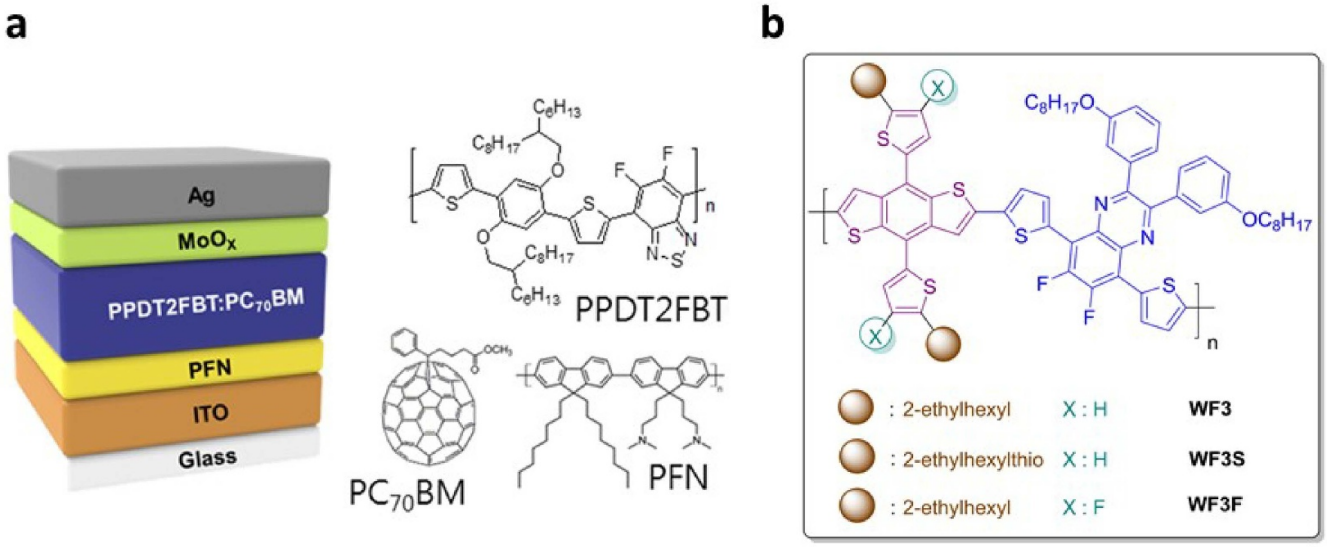

Figure 5. (a) Device structure of PPDT2FBT:$PC_{70}BM$-based inverted OPVs and chemical structures. Reprinted from [58], copyright (2019), with permission from Elsevier. (b) Chemical structures of the polymers. Reprinted with permission from [57]. Copyright (2019) American Chemical Society.

showed thickness independent performances, which could be attributed to the low electronic disorders [55]. Such properties are very critical for future mass production.

Similarly, Shin *et al* performed an in-depth investigation on the influence of the thickness of active layers on photovoltaic characteristics under indoor lights, including LEDs, FTs, and halogen lamps. A semi-crystalline polymer, poly[(2,5-bis(2-hexyldecyloxy)phenylene)-alt-(5,6-difluoro-4,7-di(thiophen-2yl)benzo[c][1,2,5]thiadiazole)] (PPDT2FBT) and $PC_{71}BM$ were used as the photoactive layer (figure 5(a)) [58]. The absorption range of PPDT2FBT is well-matched with the emission spectra of an artificial indoor light source, such as an LED. In particular, PPDT2FBT exhibits a high hole mobility of 3.0×10^{-3} cm^2 V^{-1} s^{-1}, and it shows outstanding photoactive performance even with a 300 nm thick photoactive layer without significant charge recombination [58]. Therefore, a thick photoactive layer can also minimize leakage currents and maximize photon absorption under indoor light conditions. The authors also considered the effects of device series resistance (Rs) and shunt resistance (R_P). A much lower Rs/R_P ratio was also obtained with a thick photoactive layer ($\geqslant$280 nm), leading to negligible decreases in the *FF* values and photocurrents under illumination from an LED. As a result, the PPDT2FBT:$PC_{71}BM$ device exhibited the best PCE of 16% and the maximum power output of 44.8 mW cm^{-2} under 1000 lux LED light [58].

In 2019, several wide bandgap donors (PDTBTBz-$2F_{anti}$, P3HT, PBDB-T, and PTB7) were blended with $PC_{71}BM$ to study the effects of spectrum matching with indoor lights, particularly LEDs [17]. A remarkable PCE of 23.1% under a 1000 lux LED was achieved. The authors used the finite-difference time-domain simulation method to understand the degree of spectral matching between the photoactive layer and light sources. The superior spectrum matching between the PDTBTBz-$2F_{anti}$ device with indoor lights resulted in an excellent power absorption ratio, thereby leading to the best performance. Furthermore, its IPV performance was observed to be better than that of an interdigitated-back-contact-based silicon photovoltaic cell (PCE of 16.3%) [17].

Singh *et al* designed and synthesized a series of conjugated polymers as electron donors comprising benzodithiophene (BDT) and 5,8-bis(5-bromothiophen-2-yl)-6,7-difluoro-2,3-bis(3-(octyloxy) phenyl)quinoxaline as a function of the BDT's thienyl substitution (alkyl (WF3), alkylthio (WF3S), and fluoro (WF3F)) to minimize voltage losses (figure 5(b)) [57]. The results demonstrated that the donor–acceptor blend, WF3F:$PC_{71}BM$, efficiently suppressed trap-assisted recombination losses. Along with the deeper HOMO of WF3F in comparison to the other two polymers with the alkyl (WF3) and alkylthio (WF3S) substituents, this material combination led to a high V_{OC}. The WF3F:$PC_{71}BM$ device also had a high shunt resistance (R_{Sh}) and low series resistances (R_S); as a result, it exhibited a high PCE of 17.34% under indoor LED light (500 lux, 0.17 mW cm^{-2}) and a PCE of 9.44% at 1 sun conditions, simultaneously. These findings verify that indoor performance can be enhanced further through fine-tuning of the polymer chemical structures [57].

In 2019, Arai *et al* used small-molecule donors BDT-2T-ID and BDT-1T-ID (figure 6(a)), which possess deep-lying HOMO energy levels, to prepare IPV devices [60]. When paired with a fullerene acceptor PNP, the small-molecule device exhibited a PCE exceeding 16% under white LED illumination and delivered high output power densities of up to 12.4 and 65.3 μW cm^{-2} at 200 and 1000 lx, respectively. The deep-lying HOMO energy levels of the donors could increase the V_{oc} values, and high photovoltage is a critical factor for achieving high efficiencies under indoor light sources [60]. In addition, high-performance organic energy-harvesting

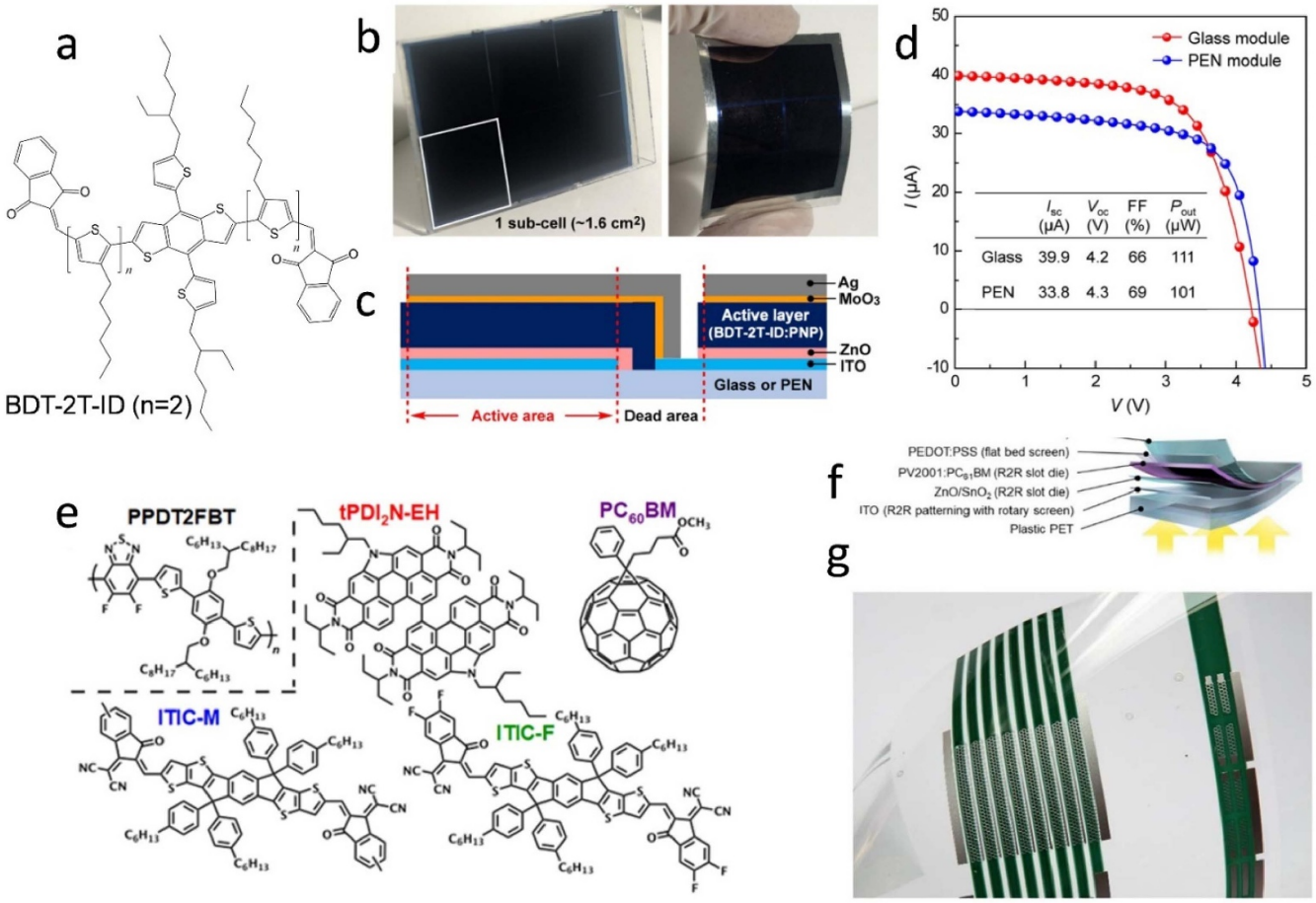

Figure 6. (a) Molecular structures of BDT-nT-IDs; (b) photographs of the BDT-2T-ID-based six series-connected modules (total active area: 9.5 cm^2) fabricated on a rigid glass substrate (left) and on a flexible PEN substrate (right); (c) schematic representation of their basic module design; (d) I–V curves for the fabricated OPV modules measured under white LED illumination at 200 lux. Reprinted with permission from [60]. Copyright (2019) American Chemical Society. (e) Chemical structures of the polymer donor PPDT2FBT and the four acceptors used in this study. Reprinted with permission from [59]. Copyright (2019) American Chemical Society. (f). Schematic representation of the OPV devices and (g) a photograph of the modules and cells in this study. Reproduced from [62]. © IOP Publishing Ltd. All rights reserved.

modules were also fabricated using both a rigid glass substrate and a flexible polyethylene naphthalate (PEN) substrate (figure 6(b)). The module design is illustrated in figure 6(c); each module comprises six series-connected subcells with a total active area of ∼10 cm^2. The module can generate a high output power surpassing 100 μW and a high photovoltage larger than 4.2 V under indoor illumination conditions at 200 lux. The results in this work reveal that indoor OPVs are promising power sources for self-sustainable electronic devices [60].

Dayneko *et al* fabricated inverted OPV devices with photoactive layers consisting of a polymer donor PPDT2FBT blended with four different acceptors, namely $PC_{60}BM$, ITIC-F, ITIC-M, and $tPDI_2N$-EH, for indoor applications using halogen-free ink formulations (figure 6(e)) [59]. Two fabrication methods, spin coating and slot-die, were used to achieve stable performance under indoor lighting conditions. The devices prepared with these blends showed PCEs of 6.5%–9.1% under 1 sun illumination and the PCE values reached efficiencies of 10%–17% under illumination from an indoor light source. The power output of the PPDT2FBT:$PC_{60}BM$ and PPDT2FBT:$tPDI_2N$-EH devices was 2.5 and two times greater than a reference Si cell under LED illuminance of 1000 lux, respectively. The cells fabricated by spin-coating and slot-die casting from nonhalogenated solvents exhibited comparable performance. This work opens a path toward high-efficiency indoor OPVs for low-power electronics [59].

In 2020, Ylikunnari *et al* prepared indoor OPV cells and modules using roll-to-roll slot-die coating and screen printing on flexible plastic substrates; the device structure was indium tin oxide (ITO)-polyethylene terephthalate (PET)/ZnO or SnO_2/PV2001:PCBM/PEDOT:PSS/silver (poly(3,4-ethylenedioxythiophene) polystyrene sulfonate (PEDOT:PSS)(figures 6(f) and (g)) [62]. The module consisted of a honeycomb structure as hole contacts, which was considered to provide sufficient conductivity for applications under low-level lighting conditions. The active areas of the cells and modules were 33 and 1360 mm^2, respectively, and each module comprised eight serially connected cells. Under 1 sun conditions, the ZnO cells and modules exhibited better

Table 2. Non-fullerene-based PV device performance under indoor light conditions.

Active layer	Light source/illumination (lux)	V_{oc} (V)	J_{SC} (mA cm^{-2})	*FF* (%)	PCE (%)	Pout (μW cm^{-2})	References
PPDT2FBT: ITIC-M	LED/300	0.53	0.0208	57	6.9	6.3	[59]
PPDT2FBT: ITIC-M	LED/1000	0.62	0.0685	54.6	7.5	23.2	[59]
PPDT2FBT: ITIC-F	LED/300	0.29	0.0348	31.3	3.5	3.2	[59]
PPDT2FBT: ITIC-F	LED/1000	0.45	0.0855	37.6	4.7	14.5	[59]
PPDT2FBT: tPDI$_2$N-EH	LED/300	0.79	0.0209	49.9	9.0	8.2	[59]
PPDT2FBT: tPDI$_2$N-EH	LED/1000	0.84	0.065	50.2	8.9	27.6	[59]
CD1: ITIC	FL/1000	0.78	0.116	68.1	17.9	62	[68]
CD1: ITIC	LED/1000	0.77	0.107	67.5	15.4	56	[68]
CD1: PBN-10	FL/1000	1.14	0.120	66.2	26.2	91	[68]
CD1: PBN-10	LED/1000	1.14	0.105	65.4	21.7	78	[68]
PBDBT-F: IO-4Cl	LED/200	1.03	0.0182	71.5	22.2	13.4	[18]
PBDBT-F: IO-4Cl	LED/1000	1.10	0.0906	79.1	26.1	78.8	[18]
PBDBT-F: IO-4Cl	LED/1000	1.07	0.089	75.3	23.9	75.3	[18]
PM6: ITCC	LED/1000	0.962	0.095	64.3	22	66.48	[41]
PM6: IT-4F	LED/1000	0.712	0.113	68.7	20.8	62.86	[41]
TPD-3F: IT-4F	FL/1000	0.75	3.98	65.1	26.2	48.5	[69]
TPD-3F: IT-4F	FL/1000	3.21	0.361	70.6	21.8	40.2	[69]
PM6:Y6-O	LED/1650	0.84	0.245	77	30.89	161.23	[70]
PBDB-TS: IT-4F	FL/500	0.36	0.0668	63.3	5.3	22.1	[67]
PBDB-TS-3Cl: IT-4F	FL/500	0.64	0.0628	73.7	20.4	60.2	[67]
PBDB-TS-4Cl: IT-4F	FL/500	0.64	0.0649	70.2	21.7	64	[67]
PM6: FCC-Cl	LED/1000	0.895	0.122	81.1	27.9	43.1	[71]
D18: FCC-Cl	LED/1000	0.955	0.123	79.8	29.4	93.5	[71]
D18: FCC-Cl-C8	LED/1000	0.947	0.11	79.3	28.4	—	[19]
D18: FCC-Cl-4Ph	LED/1000	0.972	0.110	79.0	29.3	—	[19]
D18: FCC-Cl-6Ph	LED/1000	0.996	0.094	69.8	22.6	—	[19]
PB3: FTCC-Br	LED/1000	0.954	0.119	80.72	30.00	91.68	[21]
PB4: FTCC-Br	LED/1000	0.953	0.115	79.78	28.65	87.59	[21]
PB2: ITCC	LED/1000	0.951	0.109	76.60	25.4	79.6	[20]
PB2: FTCC-Br	LED/1000	0.943	0.123	81.1	30.2	94.7	[20]
D18: Cl-BTA5	LED/1000	1.019	0.0911	68.96	21.20	—	[72]

performance. However, the encapsulated SnO_2 samples exhibited higher indoor light-harvesting properties with a PCE of up to 13.5% in cells and 13.4% in modules. The authors concluded that that SnO_2 nanoparticle (NP) ink was an alternative material for the ZnO NP ink as an electron transport material for indoor solution-processed OPV devices [62].

4.1.2. Non-fullerene materials systems. NF acceptors have received much attention recently, and record-high PCE values under standard 1 sun conditions have been achieved using this newly developed type of material. Many NF materials have also been used for developing indoor OPV devices. Their performance is summarized in table 2. In 2019, Cui *et al* demonstrated 1 cm^2 OPV cells with a top PCE of 22% under illumination from an LED (2700 K) at 1000 lux [41]. They adopted a wide-bandgap polymer donor, poly[[4,8-bis[5-(2-ethylhexyl)-4-fluoro-2-thienyl]benzo-[1,2-b:4,5-b$^{\prime}$]dithiophene-2,6-diyl]-2,5-thiophenediyl-[5,7-bis(2-ethylhexyl)-4,8-dioxo-4H,8H-benzo[1,2-c:4,5-c$^{\prime}$]-dithiophene-1,3-diyl]-2,5-thiophenediyl](PBDB-TF), and an NF acceptor, 3,9-Bis(2-methylene-(3-(1,1-dicyanomethylene)-indanone))-5,5,11,11-tetrakis(4-hexylphenyl)-dithieno[2,3-d:2',3'-d']-s-indaceno[1,2-b:5,6-b']-dithiophene) (ITCC), to make a good match with the emission spectrum of a warm white LED light. The other two electron acceptors, including a fullerene derivative acceptor $PC_{71}BM$ and a low-bandgap NF acceptor IT-4F, were also used to construct indoor OPV devices. Compared to ITCC, these two acceptors showed relatively larger photovoltage losses (V_{loss}s) and, thus, lower PCEs due to their lower-lying LUMOs. These results indicate that good matching between the absorption spectra of the photoactive layers with the emission spectra of indoor light sources and low V_{loss}s are the key factors for achieving high-performance indoor OPV devices. This work also revealed that the intensities of weak indoor light sources are of great importance in determining the PCEs of OPV devices. Therefore, an accurate evaluation of light measurement using precision lux meters and spectrometers to correctly evaluate the cell performance was required to reduce errors [51, 66]. Finally, the device stability was also evaluated under continuous illumination at different light intensities in the air. The devices suffered a fast decrease of PCEs under strong light; only less than 15% of the original PCEs were recorded after 160 h. However, the devices under weak light illumination showed impressive stability; over 90% of the original PCEs could still be obtained after 500 h, suggesting good suitability in both efficiency and stability for indoor applications [41].

Je *et al* investigated the chlorination effects of polymer donors on IPV performance [67]. As shown in figure 7(a), the

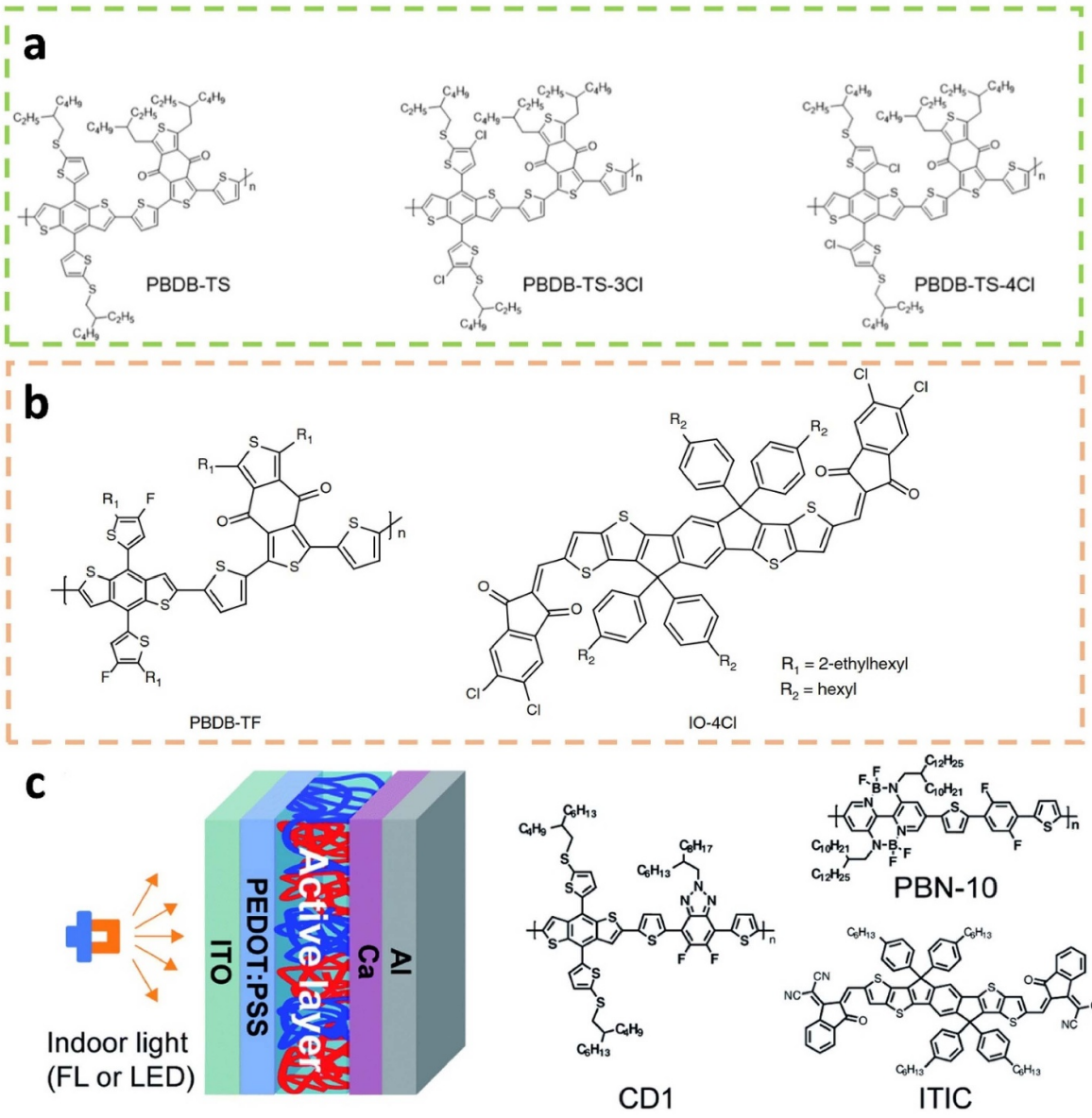

Figure 7. (a) Chemical structures of the PBDB-TS, PBDB-TS-3Cl, and PBDB-TS-4Cl polymers. Reprinted with permission from [67]. Copyright (2020) American Chemical Society. (b) Molecular structures of PBDB-TF and IO-4Cl. (c) The device architecture of IPVs under indoor light illumination and the chemical structures of CD1, PBN-10, and ITIC. Reproduced from [68] with permission from the Royal Society of Chemistry.

polymer donors PBDB-TS, PBDB-TS-Cl, and PBDB-TS-4Cl have the same thiophene-substituted benzodithiophene (BDT-Th) moiety, but chlorine atoms are substituted at different positions in the side chains. The OPV devices were fabricated using the three different polymers in conjunction with the NF acceptor, IT-4F. The chlorination increased the PCE from 8.7% (PBDB-TS:IT-4F device) to 12.6% and 12.7% for the OPV cells prepared with PBDB-TS-3Cl and PBDB-TS-4Cl, respectively, under 1 sun illumination conditions. Under illumination from a fluorescent lamp at 500 lux, the PBDB-TS:IT-4F device exhibited a very low PCE of 5.3%. However, the PCE values were increased remarkably to 21.7% and 20.4% for the PBDB-TS-4Cl:IT-4F and PBDB-TS-Cl:IT-4F devices, respectively. Under low-level lighting conditions, the photon density that reached the photoactive film was low. Therefore, harvesting the photons and converting as many of them as possible to free charge carriers is important. The authors concluded that efficient photon harvesting and charge generation were key to achieving high performance under low-intensity illumination conditions [67].

To enlarge the output photovoltage, the energy loss of OPV cells should be as low as possible [18]. The use of organic materials possessing wider E_g values can reduce E_{loss}, thereby achieving high PCE values for indoor applications. In 2019, Cui *et al* designed an acceptor–donor–acceptor (A–D–A)-structured small-molecule acceptor, IO-4Cl, which exhibited a wide optical bandgap of 1.80 eV, for constructing indoor OPV devices (figure 7(b)) [18]. Blending IO-4Cl with a polymer

donor, PBDB-TF, the OPV device (device area: 1 cm^2) demonstrated a PCE of 9.80% with a V_{oc} of 1.24 V under the standard AM 1.5G conditions. Under irradiation from an LED (2700 K) at 1000 lux, the cell achieved a PCE of 26.1% with a V_{oc} of 1.10 V. Furthermore, by adding a 1000 Ω external resistor in series, the PCE remained almost constant and retained 65% of its initial value under the 10 000 Ω condition. As a result, the authors demonstrated that the possible parasitic R_s caused by the transparent electrodes of a large-area module is not a limiting factor for indoor applications. Therefore, a large-area cell (4 cm^2) fabricated through a blade-coating method showed a PCE of 23.9% with a V_{oc} of 1.07 V [18]. Finally, the NF device showed remarkable stability under continuous low-light illumination conditions and could maintain its initial photovoltaic performance for 1000 h [18].

Among various types of organic solar cells, all-polymer photovoltaics, which use a blend of a polymer donor and acceptor as the active layer, possess the great merits of superior flexibility, stretchability, and mechanical properties. Ding *et al* employed a blend of a polymer acceptor containing boron–nitrogen coordination bonds with a bandgap of 1.95 eV (PBN-10) and another polymer donor (CD1) with a bandgap of 1.93 eV as the active layer to fabricate indoor all-polymer photovoltaic devices (figure 7(c)) [68]. The device's structure is displayed in figure 7(c). Compared with the CD1:ITIC-based device, the CD1:PBN-10-based device exhibited a lower J_{sc} under standard 1 sun illumination (AM 1.5G) but comparable J_{sc} under indoor light illumination. However, the CD1:PBN-10-based device exhibited much higher V_{oc} than that of the CD1:ITIC-based device under indoor light illumination. Although the CD1:PBN-10-based device only exhibited a low PCE of 7.9% under 1 sun illumination, it showed a high efficiency of 27.4% and a high V_{oc} of 1.16 V under indoor artificial lighting sources [68].

4.1.3. The ternary strategy. Unlike binary blends for conventional BHJ devices, ternary OPVs refer to the cells having three organic semiconductors in the active layers [73–75]. Ternary blends can consist of one donor and two acceptors, or two donors and one acceptor in a single active layer. Constructing ternary OPVs is an effective way to solve many problems that binary devices may encounter since they can improve performance: (i) enhanced carrier mobilities improve *FF*s; (ii) complementary optical absorption increases J_{sc} values; and (iii) matched energy levels enlarge V_{oc} values [66]. In 2018, Yin *et al* used several polymers as the components of ternary blends to improve the performance of PCDTBT:PC_{71}BM devices under both standard 1 sun irradiation and indoor lighting conditions [66]. The binary PCDTBT:PC_{71}BM cell exhibited a PCE of 16.5% under illumination from an FT (2700 K) at 300 lux. A polymer, PDTSTPD, which consists of a low HOMO (5.6 eV), was selected as the third component of the ternary blend. One problem with the BHJ of PCDTBT:PC_{71}BM is its relatively poor hole transport. After adding PDTSTPD, the PCE was enhanced to 20.8%, supporting the success of the ternary strategy for indoor OPV devices. The authors found that the values of *FF*s were the primarily improved factor in the ternary devices; hole mobility was increased and shallow traps near the band edges were passivated through blending the PDTSTPD as the ternary component [66, 76].

Later, Nam *et al* performed a comparative study on two donors one acceptor (2D:1A) and one donor two acceptors (1D:2A) ternary blends; they found that both approaches were universally effective for indoor and outdoor operation [77]. Figure 8(a) shows the chemical structures of the organic donors and acceptors used in the ternary blends. Their corresponding energy levels are illustrated in figure 8(b). The third components, including PTB7-Th (D_2) and ITIC-Th (A_2), both exhibited absorption at longer visible wavelengths between 600 and 800 nm, extending the absorption range of the original blend (D_1:A_1). The OPV devices were prepared using an inverted device structure (ITO/ZnO/active layer/MoO_3/Ag). The reflectance (1-R) spectra (figures 8(d) and (e)) of the two ternary devices also clearly show that the absorption spectra extend to the NIR wavelength region with increasing PTB7-Th or ITIC-Th content. For the 2D:1A devices, the optimum PCE of 18.9% was obtained when a small amount of PTB7-Th (10%) was blended (1000 lux from an LED). Although the strategy of ternary blending is effective, the overall performance depends to some extent on the spectral overlap between the absorption spectrum of the active layer and the emission spectrum of the light source. For the 1D:2A ternary devices, the optimum PCE was 22.7%. It was also found that the V_{oc} was the factor with greatest improvement in the 1D:2A device. The best 1D:2A ternary OPV exhibited a new record PCE of 26.4% at 1000 lux. From the morphology study, it was found that the A_2 molecules optimized the molecular packing and arrangement and formed favorable cascade ternary junctions, facilitating lesser charge recombination. Therefore, higher values of V_{oc} and PCE were obtained compared with binary devices [78].

Benzotriazole (BTA)-based acceptors were first reported by Zhou's group [79]; a molecular structure, A2A1DA1A2, was synthesized, where rhodanine, BTA, and indacenodithiophene were adopted as the A2, A1, and D segments, respectively. After blending with P3HT, the resulting P3HT:BTA1 device exhibited a high V_{oc} of 1.02 V and a PCE of 5.24%, which is among the highest PCE values for the OPVs prepared with P3HT:NF acceptor material combinations [79]. High V_{oc} values are usually associated with relatively low photocurrents and external quantum efficiency (EQE) values of <70% [79–81]. Because the OPVs prepared with BTA-based acceptors exhibit high V_{oc} values, this new class of acceptors is attractive for indoor applications. In particular, the introduction of a third component that has suitable energy levels to form an energy cascade alignment with the binary system leads to an increase in V_{oc} values.

In 2021, Bai *et al* adopted wide-bandgap ternary blends consisting of a BTA-based polymer donor (J52-F), a chlorinated polymer donor (PM7), and an $A_2A_1DA_1A_2$-structured acceptor (BTA3) to prepare OPVs for indoor light applications [82]. The ternary strategy was effective: the E_{loss} of the

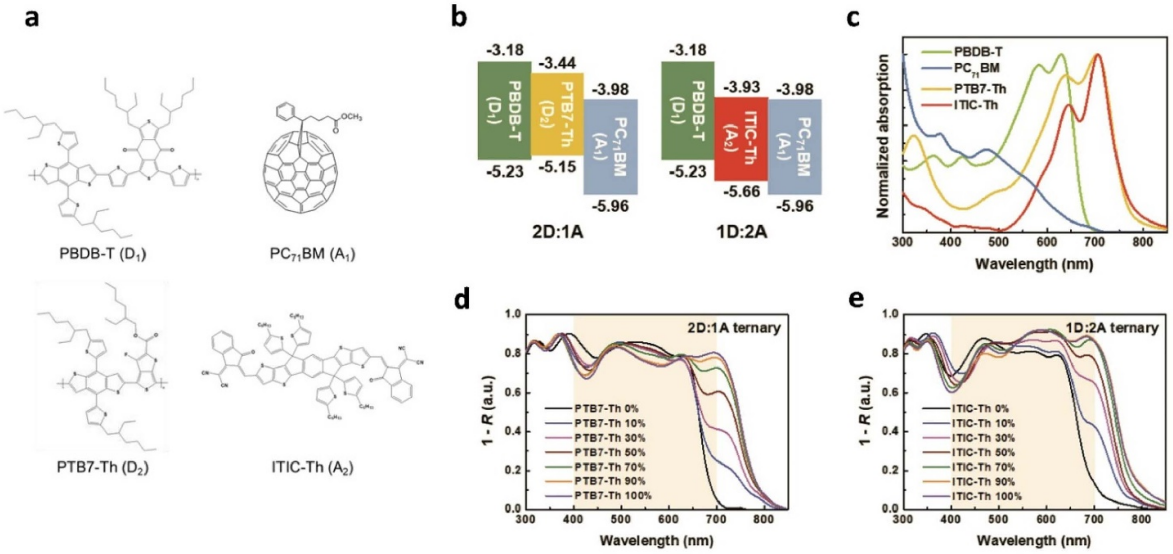

Figure 8. (a) Molecular structure of the polymer donors, fullerene ($PC_{71}BM$) and nonfullerene (ITIC-Th) acceptors. (b) Energy levels of 2D:1A or 1D:2A ternary blends incorporating additional donor (D2) of PTB7-Th or acceptor (A2) of ITIC-Th in a PBDB-T:$PC_{71}BM$ (D1:A1) blend. (c) Normalized UV–vis absorption spectra of four active layer materials. 1-R spectra of the (d) 2D:1A OPV devices as a function of PTB7-Th content and (e) the 1D:2A OPV devices as a function of ITIC-Th content. The gray colored area in insets (d) and (e) indicates the main emission region of common indoor light sources such as LEDs, FTs, etc. [77] John Wiley & Sons. © 2019 WILEY-VCH Verlag GmbH & Co. KGaA, Weinheim.

ternary device (J52-F:PM7:BTA3 = 0.9:0.1:1) was reduced to 0.62 eV, and the device V_{oc} reached 1.00 V under illumination from an indoor LED. The *FF* of the ternary device under indoor light illumination was 68.07%, which was higher than the value (61.73%) measured under AM 1.5G conditions. As a result, a high PCE of 20.04% was achieved [82]. By using NF acceptors of BTA3, the OPVs also exhibited a high PCE of 18.0% under AM 1.5G illumination conditions and a very high PCE value of 28.5% under illumination from an LED at 1000 lux [81]. Similar observations have been reported in all-polymer ternary blends [83]. For example, the V_{oc} of PTB7-Th:PNDI(2OD)-2T devices increased upon addition of PBDD-ff4T, which was attributed to the formation of an energy cascade alignment between the components [83].

4.2. Effects of the interlayers

In 2011, Steim *et al* investigated the effects of the shunt resistance (R_P) and series resistance (R_S) of OPV devices on their indoor and outdoor performances [52]. The authors first studied device performance through numerical simulations. Under 1 sun illumination conditions, they found that a high value of R_s deteriorated the performance significantly, whereas the value of R_p apparentlydid not affect the device. In contrast, the impact of R_s on the *J–V* characteristics was negligible under indoor lighting at 1000 lux, but the *FF* and V_{oc} were affected when decreasing the value of R_p. Then, P3HT:PCBM devices possessing various values of R_p were prepared and the device with the highest shunt resistance exhibited the highest power output at 1000 lux. They concluded that higher R_PA (>85 kΩ cm^2, where *A* stands for the device area) under indoor conditions (1000 lux) was crucial for achieving better device performance: because the photocurrent of IPVs is much lower, it is very important to increase the R_p of a device to minimize current loss.

In 2016, Lechêne *et al* deposited ethoxylated polyethylenimine (PEIE) with various thicknesses (thin, medium, and thick) on the active layers of indoor OPV devices to control the shunt resistances for indoor applications [84]. PEIE is an insulator and has also been shown to significantly influence the saturation dark current at reverse biases (figure 9(a)). The shunt resistances, as extracted from the dark *J–V* characteristics, were 3.3, 32, and 500 kΩ cm^2 for the thin, medium, and thick devices, respectively. As shown in figure 9(a), the PCE values for the thin and medium devices declined when the light intensity was less than 10 mW cm^{-2}. On the other hand, the thick device did not show significant decline in PCEs, even when the light fell as low as 10 μW cm^{-2}. The results revealed that surface modification using PEIE could effectively improve the performance of indoor OPV devices [84].

In 2018, Goo *et al* also used PEIE to prepare inverted devices for indoor applications [85]. Figure 9(b) displays the structure of the indoor OPV device and the materials for the active layers. The photovoltaic performance under low-level lighting conditions was optimized by controlling the thickness of the PEIE layers. Although the device showed a low PCE of 3.1% under 1 sun illumination owing to the insulating nature of PEIE, it exhibited a high PCE of 13.9% under an LED light at a luminance of 500 lux, suggesting that a sufficiently large R_PA value was of utmost importance in maximizing the PCE values under indoor lighting conditions [85]. More interestingly, Goo *et al* employed a low-cost undoped ZnO film as the TCE for their OPV devices [86]. Using atomic layer deposition, potentially defect-free and crystalline ZnO

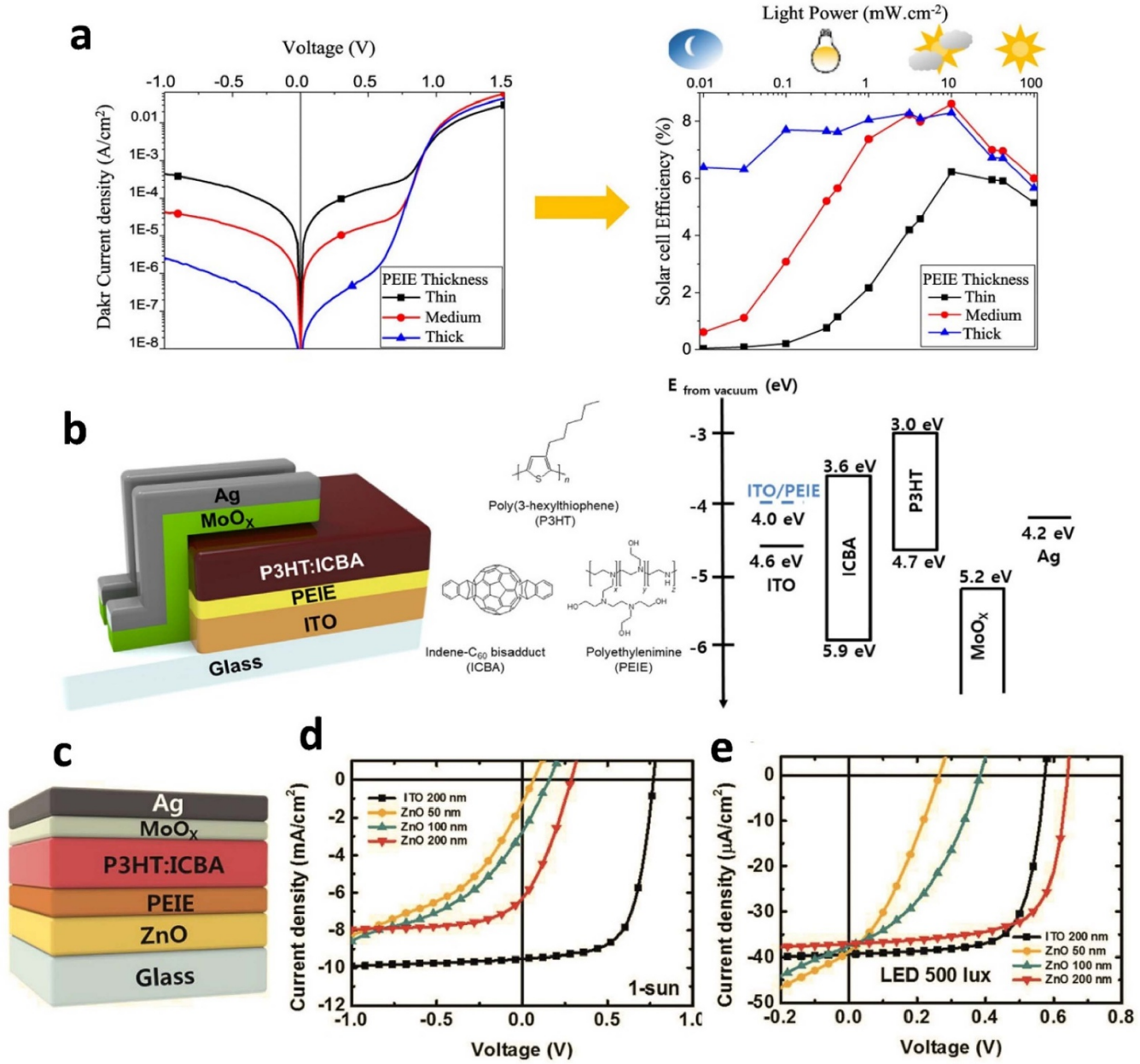

Figure 9. (a) J–V characteristics of three cells prepared with varying PEIE thicknesses measured in dark conditions and under indoor lighting conditions. Reprinted from [84], copyright (2016), with permission from Elsevier. (b) Device structure of a P3HT:ICBA-based OPV with a PEIE-modified ITO electron-collecting electrode; chemical structures of P3HT, ICBA, and PEIE; energy level diagram of the components of the OPV. Reprinted from [85], copyright (2018), with permission from Elsevier. (c) Device structure of a P3HT:ICBA-based OPV with a ZnO electrode; representative J–V characteristics of the OPVs evaluated (d) under 1 sun illumination and (e) an LED lamp (500 lux). Reproduced from [86] with permission from the Royal Society of Chemistry.

films were produced to replace conventional ITO electrodes (figure 9(c)). The device showed very poor performance under 1 sun illumination conditions because the undoped ZnO layer did not have sufficient conductivity; the sheet resistance (R_{sh}) of the ZnO film (200 nm) was as high as 260 Ω sq^{-1} and a 50 nm thick ZnO even exhibited a considerably large R_{sh} value of 4150 Ω sq^{-1} (figure 9(d)). On the other hand, the OPV device exhibited a PCE of 9.5 ± 0.3% under illumination from an LED at 500 lux (figure 9(e)). The PCE was slightly higher than or comparable to that of the reference one containing a 200 nm thick ITO TCE. A previous report revealed that ITO films account for approximately 24% of the total cost of an OPV device [87].

In 2022, Jahandar *et al* proposed a metal-mediated cross-linked nonconjugated polymer interfacial layer (c-PEIE) to suppress the voltage drop of ternary OPVs and to improve the device performance and stability of flexible OPVs from the cell-to-module scale [88]. The photoactive layer consisted of PM6:Y6:$PC_{70}BM$ (1:1:0.2). Nonconjugated polyelectrolytes such as polyethyleneimine (PEI) and PEIE widely serve as

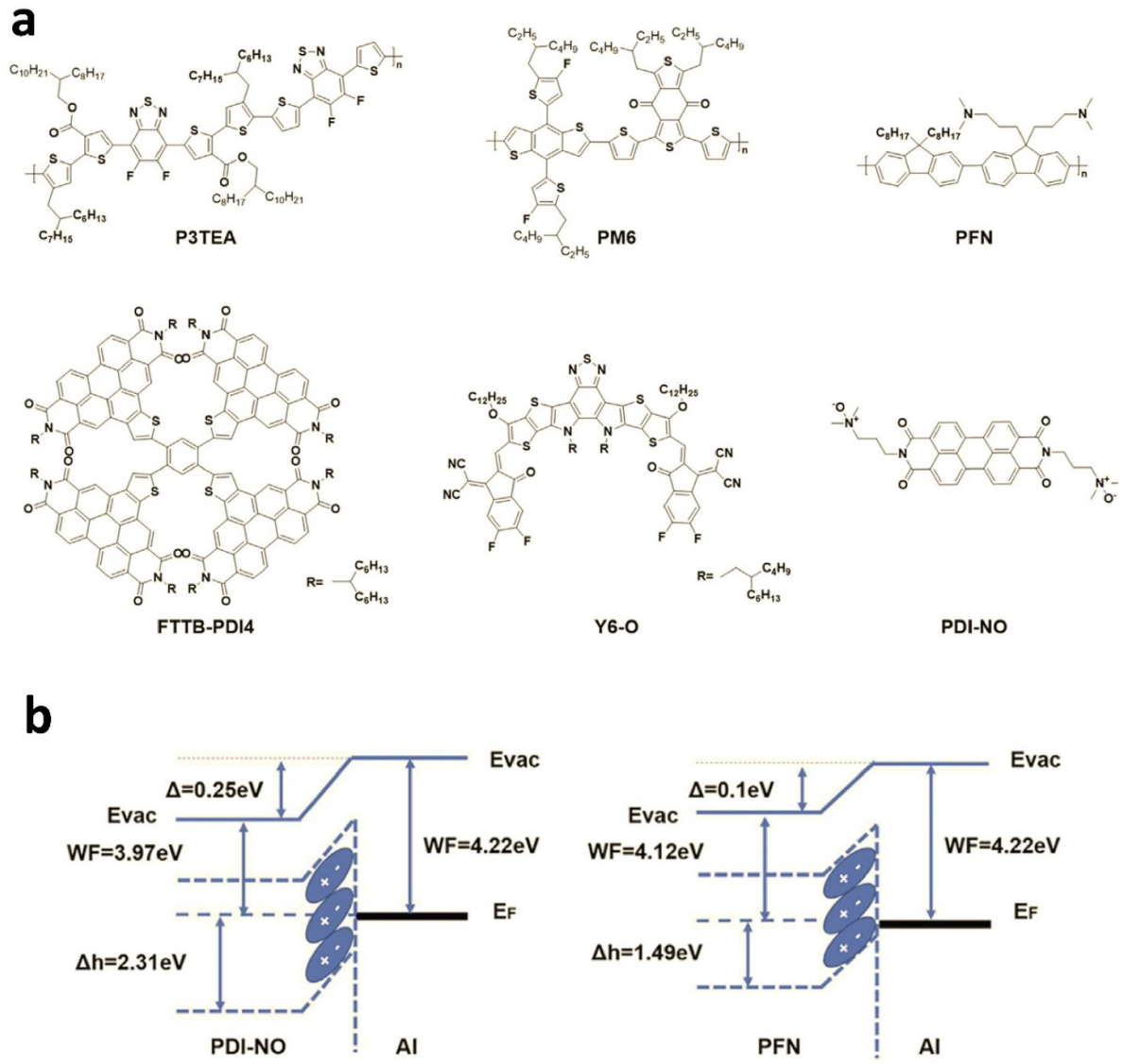

Figure 10. (a) Molecular structures of the donor polymers P3TEA, PM6, small-molecule acceptors FTTB-PDI4, Y6-O, and electron transport layer (ETL) materials PFN, and PDINO in this study. (b) Energy level alignments of ETL/Al, representing the band-bending phenomenon. Reprinted from [70], copyright (2020), with permission from Elsevier.

interlayers for OPVs. Unfortunately, an undesirable interaction between NF acceptors and PEIE hampers the development of nonconjugated polyelectrolytes for NF acceptor-based OPV devices. The use of c-PEIE could suppress the interaction between PEIE and the acceptors, thereby allowing the use of nonconjugated polyelectrolytes for these kinds of OPV devices. The flexible module exhibited a PCE of 7.41% with a P_{max} of 2.23 W (V_{oc} of 17.12 V, J_{sc} of 1.13 mA cm^{-2}, and FF of 0.38). The outdoor measurement of the 10 $\times$ 10 cm^2 flexible module for day to night under relatively low natural light conditions indicated that the module with c-PEIE performed better by having higher device voltage than the non-cross-linked injection layer. Such energy sources could provide power efficiently all day long in low-light or cloudy environments [88].

Because indoor OPV devices are not very sensitive to series resistances, replacing the ITO TCE with low-cost ZnO films can significantly reduce the overall costs [86]. After understanding the unique properties of indoor OPV devices, Lee *et al* also reported flexible devices prepared on PET substrates [89]. The quasi-amorphous ZnO/Ag/ZnO electrodes provided excellent mechanical flexibility. A P3HT:ICBA device with a ZnO/Ag/ZnO (40/9/50 nm) electrode yielded an averaged PCE of 12.3% under an LED lamp at a luminance of 500 lux and the PCE was 20% greater than that of the reference cell with an ITO electrode. The microcavity effect further enhanced light absorption. The same device fabricated on flexible PET substrates exhibited averaged PCE values of 10.2% and excellent mechanical stability [89].

In 2020, Ma *et al* focused on the role of electron-transporting layers in OPV devices under low power light illumination [70]. The authors selected two NF material systems: (1) a donor polymer PM6 with a low bandgap small-molecule acceptor (SMA), Y6-O; and (2)

a donor polymer P3TEA with a wide bandgap SMA, FTTB-PDI4 (figure 10(a)). Two different interlayers, 2,9-Bis[3-(dimethyloxidoamino)propyl]anthra[2,1,9-def:6,5,10-d'e'f']diisoquinoline-1,3,8,10(2H,9H)-tetrone (PDINO) and poly[(9,9-bis(3'-(N,N-dimethylamino)propyl)-2,7-fluorene)-alt-2,7-(9,9-dioctylfluorene)](PFN), were used to prepare the devices (figure 10(a)) [70]. The HOMO levels of PDINO and PFN were −6.21 and −5.61 eV, respectively. Although the performance of the two different OPV devices was very similar under 1 sun irradiation, they exhibited different device behavior under indoor lighting conditions. As shown in figure 10(b), the energy alignment between interlayers and the Al electrode was investigated by ultraviolet photoelectron spectroscopy. The work function (WF) shifted from 4.22 to 4.12 eV upon Al modification with PFN and shifted from 4.22 to 3.87 eV with PDINO. Both interlayers reduced the WF values, thereby facilitating the formation of ohmic contacts and increasing the built-in potential inside the devices. However, the difference between the HOMO and Fermi level (which is related to the hole injection/extraction barrier) of the PDINO (−2.31 eV) case was higher than that of the PFN (−1.49 eV) devices. As a result, we can expect that the PDINO interlayer would provide better hole-blocking ability. Under 1 sun conditions, the PCE values of the PM6:Y6-O devices prepared with PDINO and PFN interlayers were 16.53% and 16.20%, respectively. The P3TEA:FTTB-PDI4 devices also exhibited similar PCE values while using PDINO and PFN as the interlayers. On the other hand, PDINO-based devices achieved significantly better performance than PFN-based devices under low-light intensity conditions. For instance, the devices based on PM6:Y6-O and PDINO interlayers exhibited a high PCE of 31% at 1650 lux, which was higher than that of the device prepared with PFN (22.47%). Further analysis indicated that PDINO-based devices exhibited lower leakage current and trap-assisted recombination under indoor lighting conditions [70].

4.3. Plasmonic nanostructures for indoor applications

The use of plasmonic structures has emerged as an effective approach for light-trapping enhancement in PVs at the nanoscale, well below the scale of the wavelength of light in free space [90, 91]. In particular, metallic nanostructures (e.g. Ag, Al, Au, Cu, etc) are the most extensively employed plasmonic structures for enhancing the performance of PV devices; they are able to enhance and/or redistribute the optical field and/or scatter light waves inside devices, thereby improving the optoelectronic properties of OPV devices [92–94]. Furthermore, various plasmonic electrodes (e.g. metallic gratings, Bragg reflectors, metamaterial mirrors) have also been designed to improve absorption in OPVs along with different implementation strategies [95]. Commonly, surface plasmon-polaritons appearing as a form of propagating light waves along a meta/dielectric interface can be excited in PVs by employing periodically nanopatterned metal films, resulting in near-field enhancement and improved optical absorption [96–98]. On the other hand, embedding metal NPs in OPVs exploits the strongly confined field of the localized surface plasmon resonance (LSPR) and achieves more efficient light absorption within the devices. Small metal NPs (usually smaller than 20 nm in diameter) can act as subwavelength antennas, in which the enhanced near-field is coupled to the absorbing OPV layer(s), thereby increasing effective absorption cross-section [99–101]. Large NPs (e.g. larger than 40 nm in diameter) can be used as effective subwavelength scattering elements that significantly increase the optical path length of the sunlight within the active layers [102]. Furthermore, tuning geometric parameters, such as the size and shape of the metal NPs, can promote interactions between longitudinal and transverse modes supported in the embedded NP arrays or clusters in the active layers.

Plasmonic nanostructures can also be adopted to improve the efficiencies of indoor OPVs [54]. As shown in figures 11(a)–(c), we previously incorporated gold NP-decorated graphene oxides (Au@PEG-GO) into the hole-transporting and active layers of OPVs to trigger plasmonic effects [54]. We found that the device PCEs were much higher under indoor light than they were under sunlight. Moreover, from theoretical calculations, the enhancement factor was slightly larger for devices under illumination from indoor light sources. Because the plasmonic band of the Au NPs is located in the visible spectral range, the better spectral overlapping with the incoming photons was larger compared to solar irradiation. Indeed, the experimental results revealed that the enhancement factors, meaning the percentage that the PCE improved after using the plasmonic NPs, were 26.8% and 20.4% for the devices illuminated with a white LED and an FT (at 1000 lux), respectively. Meanwhile, the factor was only 17.5% for the device illuminated with 1 sun. The results strongly indicate that the plasmonic strategy is more suitable for indoor OPVs because the emission spectra of the light sources are much narrower than that of solar irradiation [54].

We have also investigated the role of copper (Cu) NPs for improving the performance of OPVs under low-power light sources [105]. Cu is more abundant, and Cu NPs also exhibit plasmonic properties in the visible wavelength range. Furthermore, their cost is much lower than that of noble metals, including Ag and Au; therefore, the effects of Cu NPs are worthy of study. Recently, Cu NPs were incorporated into PBDTTT-EFT:$PC_{71}BM$ devices and the PCE values were apparently improved. Under illumination from an FT at 200 lux, the PCE was increased from 11.30% to 12.53%; the PCE was also improved from 12.15% to 12.65% at 600 lux. The enhancement in device performance was even higher when the indoor light source was a white LED. The PCE was increased from 11.15% to 13.11% at 200 lux. When the luminance was 600 lux, the efficiency was improved from 12.08% to 13.52%. The best device exhibited a PCE of 14.31% at 500 lux. The higher enhancement factor under illumination from a white LED could be attributed to larger overlapping between the LSPR band of the Cu NPs and the emission spectrum of the white LED. Therefore, we concluded that the spectral matching between the plasmonic resonance range and the emission spectra of the artificial light sources is very critical to the performance of indoor OPVs [105].

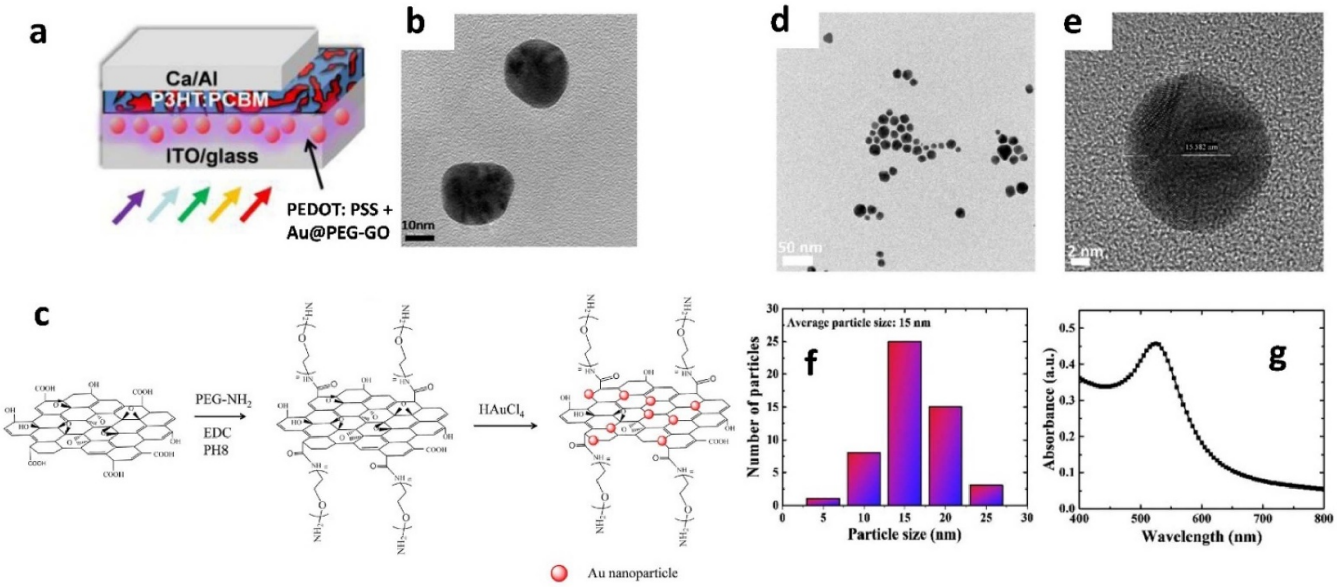

Figure 11. (a) Structure of OPV devices prepared for plasmonic enhancement. Reprinted with permission from [94]. Copyright (2013) American Chemical Society. (b) Transmission electron microscopy (TEM) image of Au NPs, and (c) schematic representations of the synthesis route for Au@PEG-GO. Reprinted with permission from [103]. Copyright (2015) American Chemical Society. (d) TEM image of Au–Cu alloy NPs; (e) high-resolution TEM image of a single alloy NP (diameter: 15.58 nm); (f) the size distribution of alloy NPs; (g) the absorption spectrum of Au–Cu alloy NPs dispersed in water. Reprinted with permission from [104] © The Optical Society.

Although Cu is an ideal metal for plasmonic materials, Cu NPs are readily oxidized and have low chemical stability. Previously, Liu *et al* modified the surfaces of Cu NPs to prevent oxidation and used the resulting NPs to improve the efficiencies of OPV devices [106]. In our previous work, we also processed Cu NPs in an inert environment to prevent their oxidation [105]. More recently, we synthesized Au–Cu alloy NPs to improve the performance of OPV devices [104]. The addition of Au element in the NPs enhanced the stability of the alloy NPs so that we could blend them with the anodic buffer solution of PEDOT:PSS and annealed the resulting thin films directly in air. As shown in figures 11(d)–(f), the average size of the alloy NPs was 15 nm and it exhibited a typical plasmonic band (525 nm; figure 11(g)), which was located between the two wavelength extremes calculated from the model assuming pure Au and Cu NPs, respectively. The active polymer blends consisted of poly[4,8-bis(5-(2-ethylhexyl) thiophen-2-yl) benzo[1,2-b;4,5-b'] dithiophene-2,6-diyl-alt-(4-(2-ethylhexyl)-3-fluorothieno[3,4-b] thiophene-)-2-carboxylate-2-6-diyl)] (PTB7-Th) and [6,6]-Phenyl-C71-butyric acid methyl ester ($PC_{71}BM$). The device performance was enhanced under indoor lighting conditions after using the alloy NPs. For example, under illumination from an FT, the values of V_{oc}, J_{sc}, and *FF* for the OPV device were 0.60 V, 28.1 μA cm^{-2}, and 0.46, respectively, resulting in a PCE of 12.0% at 200 lux. After integrating NPs in the device, the J_{sc} and *FF* were increased to 30 μA cm^{-2} and 0.56, respectively, leading to an improved PCE of 14.9%, suggesting their suitability for indoor applications [104].

4.4. Module fabrication and system integration

The development of industrial manufacturing methods for OPV modules is still very challenging. Many issues involving the scalability of materials synthesis and implementability of large-area modules still have to be addressed. Furthermore, the fabrication of many record efficiencies of OPV devices relies on using halogenated solvents as processing solvents (e.g. chlorobenzene and chloroform), which are harmful to human health and the environment [69]. To overcome these problems, Liao *et al* reported the realization of readily accessible donor polymers (named for simplicity TPD-*n*, n = 1–3, 3F; figure 12(a)) and their implementation in high-efficiency solar cells and modules processable from halogen-free solvents [69]. The HOMO levels of TPD-series polymer donors are suitable for photoinduced charge separation using IT-4F as the electron acceptor; for instance, the TPD-3F:IT-4F blend possessed a very low energy of HOMO difference (0.04 eV), which ensured a high V_{oc} value. The structure of the OPV devices was glass/ITO/ZnO/TPD-*n*:IT-4F/MoO_3/Ag. Among the combinations of the polymer donors and IT-4F, the TPD-3F:IT-4F cells fabricated using o-Xylene (a halogen-free solvent) with an antireflection coating exhibited a high PCE of 14.4% and the certified PCE value was 14.2%. OPV modules were then fabricated using o-Xylene as the processing solvent in ambient conditions and a module consisting of five (stripe) subcells monolithically integrated and connected in series by ITO-to-Ag interconnects; the effective area was 5.95 cm^2 per cell. A certified PCE of 10.08% under 1 sun

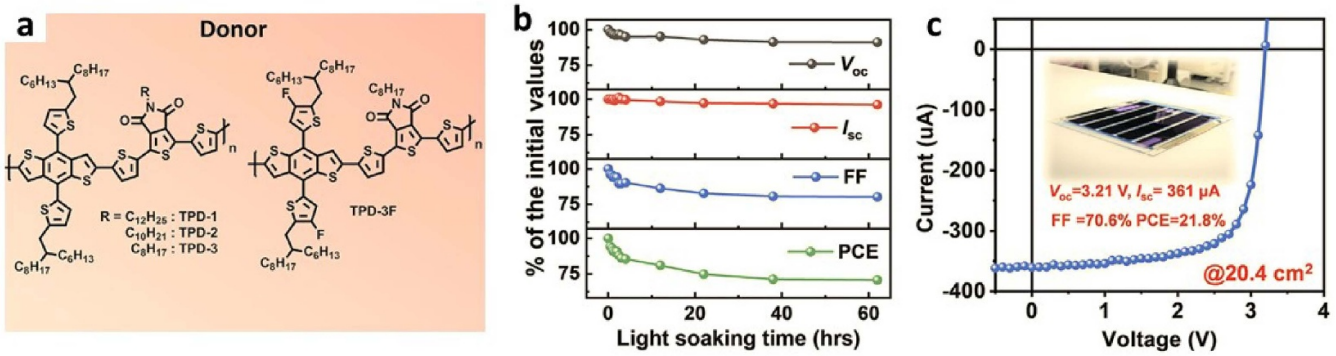

Figure 12. (a) Chemical structures of the TPD polymers employed in this study. (b) Module stability test under light-soaking conditions (initial PCE = 9.84%) and (c) representative J–V characteristics of the TPD-3F-51K:IT-4F module under a fluorescent lamp with a luminance of 1000 lux. Reprinted from [69], copyright (2020), with permission from Elsevier.

illumination conditions was obtained for the module fabricated by spin-coating, and the large module exhibited only a ∼20% cell-to-module loss. The other module fabricated by blade-coating exhibited statistically an identical PCE value of 10.40%. Light-soaking stability tests for the module are illustrated in figure 12(b); the initial PCE of the module was 9.84%. The results suggest that the module exhibited stable performance after an initial loss, and a PCE of ∼7.1% was retained. The module stability indicates that the OPV technology is promising for achieving commercial entry [69]. More importantly, the best cell and module were tested with a FT (1000 lux; TL84). The output powers of the cell and module reached 48.5 and 40.2 mW cm^{-2}, respectively, which correspond to PCE values of 26.2% and 21.8%, respectively.

Moreover, many modules for indoor applications have also been reported. For example, as discussed above, energy-harvesting modules were fabricated both on rigid glass substrates and a flexible PEN substrate (figure 6(g)) [60]. These results support that indoor OPVs could be promising power sources for future electronic systems [25, 107, 108]. Moreover, as a proof-of-concept for indoor applications, modules were combined with fully printed super-capacitors to form a photo-rechargeable systemthat can generate and store energy simultaneously [84]. The super-capacitors consisted of a gel polymer electrolyte sandwiched between composite carbon electrodes. The integrated system with a 0.475 cm^2 indoor-optimized OPV cell could deliver an energy conversion and storage efficiency of 2.9%, providing 13.3 mJ of energy and a power output of 2.8 mW under simulated indoor light conditions. The system was charged under indoor light (0.31 mW cm^{-2}) for 3090 s and provided energy and power levels similar to the 1 sun scenario [84].

5. Challenges

Although OPV technology has made significant progress over the past few years, there are still several challenges that need to be addressed before OPVs become widely adopted devices. The challenges include:

(1) Efficiency: while OPV cells exhibit higher efficiency under dim-light conditions, they may still struggle to provide sufficient power to directly drive most electronics for indoor applications. Therefore, continuous improvement in PCEs is still required, and some light-concentration technology could be also useful.
(2) Stability: although the stability issue is less critical for indoor applications, OPV devices are still unstable compared to traditional inorganic solar cells. We also have to pay more attention to factors affecting device stability, such as photodegradation and thermal degradation [109], which limit a device's long-term performance and reliability [110].
(3) Cost: while OPVs have the potential to be low-cost, production of high-performance OPV devices is still relatively expensive, especially in the early stages of commercialization.
(4) Device design: the design of OPV devices could be complicated and requires the optimization of multiple factors, including the morphology of the active layers, the selection of the active materials, and the design of the device's structure [111]. This complexity can make the development and optimization of OPV products very challenging.
(5) Environmental impact: although the environmental impact of OPVs is usually considered much less compared to inorganic counterparts, it should still be carefully evaluated.

Overall, the development of indoor OPV technology presents both opportunities and challenges, and ongoing research and development efforts are needed to optimize their performance, stability, and scalability.

6. Summary and perspective

Indoor OPVs have great potential for powering many indoor appliances, including IoT ecosystems, sensors, wearable electronics, and communication devices. In particular, indoor OPV devices provide much higher performance than traditional

Si-based devices under indoor and/or low-level lighting conditions. The optoelectronic properties of photoactive organic materials such as their bandgaps and absorption spectra can be finely tuned to match the emission spectra of common indoor light sources to improve their efficiencies. Their low fabrication cost could trigger higher demand for IPV devices and inspire an even wider range of applications.

However, there are still some key issues that have to be addressed. (1) The understanding of energy loss (E_{loss}) for indoor applications is lagging behind that of regular solar cells. Under illumination at lower light intensity, the changes in device characteristics also require further clarification. (2) In addition to the energy levels and bandgaps, more design rules are still required for indoor OPV materials. (3) Under indoor lighting conditions, light intensity and temperature are relatively low. Therefore, it is generally agreed that OPV devices exhibit better stability under indoor operating conditions. However, there are still very few studies in the literature investigating the stability of indoor cells and modules. Standard assessment procedures for evaluating stability for indoor uses must be established. (4) Standardization of indoor measurements is another issue. The standards for light emission, light intensity, and measurement protocols have not yet been established. It is very important to accurately evaluate the photovoltaic performance and enable a fair comparison between results obtained from different laboratories. (5) Apparently, there is still room for improvement in indoor PCE values. The development of new materials that can match the properties of indoor lighting sources is still necessary. The development of new light-harvesting schemes is also very important. For example, many plasmonic bands of metal NPs are located in the visible spectral range, which exactly match the emission spectra of indoor light sources. Considerable plasmonic effects are expected, and the performance enhancement should be very significant compared to outdoor solar cells. Therefore, the strategy of using metal NPs for improving performance will be very useful for indoor OPV applications.

In summary, indoor OPV cells have achieved rapid progress recently. Because the modules are less sensitive to series resistances, transparent electrodes with lower costs (higher series resistances) could be suitable for commercial products. Replacing ITO films with low-cost electrodes could reduce the cost significantly. With further improvements in efficiencies and stability, we believe low-cost, highly efficient OPV modules for indoor applications will be realized very soon.

Data availability statement

No new data were created or analyzed in this study.

Acknowledgments

This work is supported by the National Science and Technology Council, Taiwan (Grant Nos. NSTC 109-2221-E-009-147-MY3, 111-2634-F-A49-007, and 111-2218-E-A49-019-MBK) and the Center for Emergent Functional Matter Science of National Yang Ming Chiao Tung University from The Featured Areas Research Center Program within the framework of the Higher Education Sprout Project by the Ministry of Education (MOE) in Taiwan.

ORCID iDs

Gautham Kumar https://orcid.org/0000-0002-5095-3331
Fang-Chung Chen https://orcid.org/0000-0002-4131-3893

References

[1] Sondergaard R, Hosel M, Angmo D, Larsen-Olsen T T and Krebs F C 2012 *Mater. Today* **15** 36
[2] Kang H, Kim G, Kim J, Kwon S, Kim H and Lee K 2016 *Adv. Mater.* **28** 7821
[3] Pandey A, Patel M S, Chaudhary D K, Patel S P, Pali L S, Garg A and Kumar L 2021 *J. Phys. D: Appl. Phys.* **54** 275502
[4] Huang Y, Kramer E J, Heeger A J and Bazan G C 2014 *Chem. Rev.* **114** 7006
[5] Yao H *et al* 2019 *J. Am. Chem. Soc.* **141** 7743
[6] Qian D *et al* 2018 *Nat. Mater.* **17** 703
[7] Ans M, Ayub A, Alwadai N, Rasool A, Zahid M, Iqbal J and Al-Buriahi M S 2022 *J. Appl. Phys.* **55** 235501
[8] Zou Y, Sun C, Xu X, Zhou Z, Luo X, Lu X, Hu Y, Yuan J and Xia X 2022 *J. Appl. Phys.* **55** 374002
[9] Liu Q *et al* 2020 *Sci. Bull.* **65** 272
[10] Asghari P, Rahmani A M and Javadi H H S 2019 *Comput. Netw.* **148** 241
[11] Wilson G M *et al* 2020 *J. Phys. D: Appl. Phys.* **53** 493001
[12] Dennler G *et al* 2007 *Sol. Energy* **81** 947
[13] Wu J L, Chen F C, Chuang M K and Tan K S 2011 *Energy Environ. Sci.* **4** 3374
[14] Cutting C L, Bag M and Venkataraman D 2016 *J. Mater. Chem.* C **4** 10367
[15] Mathews I, Kantareddy S N, Buonassisi T and Peters I M 2019 *Joule* **3** 1415
[16] Russo J, Ray W and Litz M S 2017 *Appl. Energy* **191** 10
[17] You Y J, Song C E, Hoang Q V, Kang Y, Goo J S, Ko D H, Lee J J, Shin W S and Shim J W 2019 *Adv. Funct. Mater.* **29** 1901171
[18] Cui Y *et al* 2019 *Nat. Energy* **4** 768
[19] Luo S W *et al* 2022 *Nano Energy* **98** 107281
[20] Zhang T *et al* 2022 *Adv. Mater.* **34** e2207009
[21] Bi P *et al* 2023 *J. Mater. Chem.* A **11** 983
[22] Wu Q *et al* 2022 *Joule* **6** 2138
[23] Chen F C 2019 *Adv. Opt. Mater.* **7** 1800662
[24] Ryu H S, Park S Y, Lee T H, Kim J Y and Woo H Y 2020 *Nanoscale* **12** 5792
[25] Lee H K H, Li Z, Durrant J R and Tsoi W C 2016 *Appl. Phys. Lett.* **108** 253301
[26] Foti M, Tringali C, Battaglia A, Sparta N, Lombardo S and Gerardi C 2014 *Sol. Energy Mater Sol. Cells* **130** 490
[27] Sariciftci N S, Smilowitz L, Heeger A J and Wudl F 1992 *Science* **258** 1474
[28] Brabec C J, Zerza G, Cerullo G, de Silvestri S, Luzzati S, Hummelen J C and Sariciftci S 2001 *Chem. Phys. Lett.* **340** 232
[29] Halls J J M, Pichler K, Friend R H, Moratti S C and Holmes A B 1996 *Appl. Phys. Lett.* **68** 3120
[30] Markov D E, Amsterdam E, Blom P W, Sieval A B and Hummelen J C 2005 *J. Phys. Chem.* A **109** 5266
[31] Markov D E, Tanase C, Blom P W M and Wildeman J 2005 *Phys. Rev.* B **72** 045217
[32] Tessler N, Preezant Y, Rappaport N and Roichman Y 2009 *Adv. Mater.* **21** 2741

[33] Fallahpour A H, Gagliardi A, Santoni F, Gentilini D, Zampetti A, Maur M A D and di Carlo A 2014 *J. Appl. Phys.* **116** 184502
[34] Choulis S A, Kim Y, Nelson J, Bradley D D C, Giles M, Shkunov M and McCulloch I 2004 *Appl. Phys. Lett.* **85** 3890
[35] Chen F C, Ko C J, Wu J L and Chen W C 2010 *Sol. Energy Mater Sol. Cells* **94** 2426
[36] Xu Z Q *et al* 2020 *ACS Appl. Mater. Interfaces* **12** 9537
[37] de Castro F A, Heier J, Nüesch F and Hany R 2010 *IEEE J. Sel. Top. Quantum Electron.* **16** 1690
[38] Nuesch F, Rotzinger F, Si-Ahmed L and Zuppiroli L 1998 *Chem. Phys. Lett.* **288** 861
[39] Kemerink M, Kramer J M, Gommans H H P and Janssen R A J 2006 *Appl. Phys. Lett.* **88** 192108
[40] Yang S S, Hsieh Z C, Keshtov M L, Sharma G D and Chen F C 2017 *Sol. RRL* **1** 1700174
[41] Cui Y, Yao H, Zhang T, Hong L, Gao B, Xian K, Qin J and Hou J 2019 *Adv. Mater.* **31** 1904512
[42] Ho J K W, Yin H and So S K 2020 *J. Mater. Chem.* A **8** 1717
[43] Minnaert B and Veelaert P 2014 *Energies* **7** 1500
[44] Chen C Y *et al* 2017 *J. Phys. Chem. Lett.* **8** 1824
[45] Manor A, Katz E A, Andriessen R and Galagan Y 2011 *Appl. Phys. Lett.* **99** 173305
[46] Li N, Lassiter B E, Lunt R R, Wei G and Forrest S R 2009 *Appl. Phys. Lett.* **94** 023307
[47] Wu M J, Kuo C C, Jhuang L S, Chen P H, Lai Y F and Chen F C 2019 *Adv. Energy Mater.* **9** 1901863
[48] Freunek M and Reindl L M 2013 *IEEE J. Photovolt.* **3** 1464
[49] National Renewable Energy Laboratory (NREL) (Washington, DC: US Department of Energy) (available at: www.nrel.gov/grid/solar-resource/spectra-am1.5.html)
[50] Khan J A, Sharma R, Panwar A S and Gupta D 2022 *J. Phys. D: Appl. Phys.* **55** 495503
[51] Lee H K H, Wu J Y, Barbe J, Jain S M, Wood S, Speller E M, Li Z, Castro F A, Durrant J R and Tsoi W C 2018 *J. Mater. Chem.* A **6** 5618
[52] Steim R, Ameri T, Schilinsky P, Waldauf C, Dennler G, Scharber M and Brabec C J 2011 *Sol. Energy Mater Sol. Cells* **95** 3256
[53] Mori S, Gotanda T, Nakano Y, Saito M, Todori K and Hosoya M 2015 *Jpn. J. Appl. Phys.* **54** 071602
[54] Teng N W, Yang S S and Chen F C 2018 *IEEE J. Photovolt.* **8** 752
[55] Yin H, Chen S, Cheung S H, Li H W, Xie Y M, Tsang S W, Zhu X J and So S K 2018 *J. Mater. Chem.* C **6** 9111
[56] Singh R, Shin S C, Lee H, Kim M, Shim J W, Cho K and Lee J J 2019 *Chem.Eur.J.* **25** 6154
[57] Singh R, Chochos C L, Gregoriou V G, Nega A D, Kim M, Kumar M, Shin S C, Kim S H, Shim J W and Lee J J 2019 *ACS Appl. Mater. Interfaces* **11** 36905
[58] Shin S C, Koh C W, Vincent P, Goo J S, Bae J H, Lee J J, Shin C, Kim H, Woo H Y and Shim J W 2019 *Nano Energy* **58** 466
[59] Dayneko S V, Pahlevani M and Welch G C 2019 *ACS Appl. Mater. Interfaces* **11** 46017
[60] Arai R, Furukawa S, Hidaka Y, Komiyama H and Yasuda T 2019 *ACS Appl. Mater. Interfaces* **11** 9259
[61] Arai R, Furukawa S, Sato N and Yasuda T 2019 *J. Mater. Chem.* A **7** 20187
[62] Ylikunnari M *et al* 2020 *Flex. Print. Electron.* **5** 014008
[63] Femia N, Petrone G, Spagnuolo G and Vitelli M 2005 *IEEE Power Electron. Lett.* **20** 963
[64] Xiao L, Chen S, Gao K, Peng X, Liu F, Cao Y, Wong W Y, Wong W K and Zhu X 2016 *ACS Appl. Mater. Interfaces* **8** 30176
[65] Chen S *et al* 2017 *J. Mater. Chem.* A **5** 25460
[66] Yin H, Ho J K W, Cheung S H, Yan R J, Chiu K L, Hao X and So S K 2018 *J. Mater. Chem.* A **6** 8579
[67] Je H I, Shin E Y, Lee K J, Ahn H, Park S, Im S H, Kim Y H, Son H J and Kwon S K 2020 *ACS Appl. Mater. Interfaces* **12** 23181
[68] Ding Z C, Zhao R Y, Yu Y J and Liu J 2019 *J. Mater. Chem.* A **7** 26533
[69] Liao C-Y *et al* 2020 *Joule* **4** 189
[70] Ma L-K *et al* 2020 *Joule* **4** 1486
[71] Bai F J *et al* 2021 *Joule* **5** 1231
[72] Wang Z, Tang A, Wang H, Guo Q, Guo Q, Sun X, Xiao Z, Ding L and Zhou E 2023 *Chem. Eng. J.* **451** 139080
[73] Ni M-Y, Leng S-F, Liu H, Yang Y-K, Li Q-H, Sheng C-Q, Lu X, Liu F and Wan J-H 2021 *J. Mater. Chem.* C **9** 3826
[74] Ma X *et al* 2021 *ACS Appl. Mater. Interfaces* **13** 57684
[75] Li X M, Duan X P, Qiao J W, Li S L, Cai Y H, Zhang J Q, Zhang Y, Hao X T and Sun Y M 2023 *Adv. Energy Mater.* **13** 2203044
[76] Anitha B, Joseph A, Alexander A, Vijith K P, Varun S and Namboothiry M A G 2022 *J. Phys. D: Appl. Phys.* **55** 125301
[77] Nam M, Kang J H, Shin J, Na J, Park Y, Cho J, Kim B, Lee H H, Chang R and Ko D H 2019 *Adv. Energy Mater.* **9** 1901856
[78] Wang C F *et al* 2017 *Nano Energy* **37** 24
[79] Xiao B, Tang A, Zhang J, Mahmood A, Wei Z and Zhou E 2017 *Adv. Energy Mater.* **7** 1602269
[80] Baran D *et al* 2016 *Energy Environ. Sci.* **9** 3783
[81] Xu Y, Cui Y, Yao H, Zhang T, Zhang J, Ma L, Wang J, Wei Z and Hou J 2021 *Adv. Mater.* **33** 2101090
[82] Bai Y, Yu R, Bai Y, Zhou E, Hayat T, Alsaedi A and Tan Z A 2021 *Green Energy Environ.* **6** 920
[83] Su W, Fan Q, Guo X, Guo B, Li W, Zhang Y, Zhang M and Li Y 2016 *J. Mater. Chem.* A **4** 14752
[84] Lechene B P, Cowell M, Pierre A, Evans J W, Wright P K and Arias A C 2016 *Nano Energy* **26** 631
[85] Goo J S, Shin S C, You Y J and Shim J W 2018 *Sol. Energy Mater Sol. Cells* **184** 31
[86] Goo J S, Lee J H, Shin S C, Park J S and Shim J W 2018 *J. Mater. Chem.* A **6** 23464
[87] Emmott C J M, Urbina A and Nelson J 2012 *Sol. Energy Mater Sol. Cells* **97** 14
[88] Jahandar M, Prasetio A, Lee C, Kim H, Kim A R, Heo J, Kim Y, Kim S and Lim D C 2022 *Chem. Eng. J.* **448** 137555
[89] Lee B R, Goo J S, Kim Y W, You Y J, Kim H, Lee S K, Shim J W and Kim T G 2019 *J. Power Sources* **417** 61
[90] Chou C H and Chen F C 2014 *Nanoscale* **6** 8444
[91] Petoukhoff C E, Shen Z Q, Jain M, Chang A M and O'Carroll D M 2015 *J. Photon. Energy* **5** 057002
[92] Wu J L, Chen F C, Hsiao Y S, Chien F C, Chen P, Kuo C H, Huang M H and Hsu C S 2011 *ACS Nano* **5** 959
[93] Kao C S, Chen F C, Liao C W, Huang M H and Hsu C S 2012 *Appl. Phys. Lett.* **101** 193902
[94] Tan K S, Chuang M K, Chen F C and Hsu C S 2013 *ACS Appl. Mater. Interfaces* **5** 12419
[95] Esfandyarpour M, Garnett E C, Cui Y, McGehee M D and Brongersma M L 2014 *Nat. Nanotechnol.* **9** 542
[96] Catrysse P B and Fan S 2010 *Nano Lett.* **10** 2944
[97] Lu D, Rengnath E, Cui Y, Wang Z, Ding Y and Park W 2013 *Appl. Phys. Lett.* **102** 241114
[98] Petoukhoff C E and O'Carroll D M 2015 *Nat. Commun.* **6** 7899
[99] Atwater H A and Polman A 2010 *Nat. Mater.* **9** 205
[100] Chen F C, Wu J L, Lee C L, Hong Y, Kuo C H and Huang M H 2009 *Appl. Phys. Lett.* **95** 013305

[101] Wang C C D, Choy W C H, Duan C H, Fung D D S, Sha W E I, Xie F X, Huang F and Cao Y 2012 *J. Mater. Chem.* **22** 1206
[102] Spyropoulos G D, Stylianakis M M, Stratakis E and Kymakis E 2012 *Appl. Phys. Lett.* **100** 213904
[103] Chuang M K and Chen F C 2015 *ACS Appl. Mater. Interfaces* **7** 7397
[104] Kumar G, Sharma G D and Chen F C 2021 *Opt. Mater. Express* **11** 1037
[105] Huang C L, Kumar G, Sharma G D and Chen F C 2020 *Appl. Phys. Lett.* **116** 253302
[106] Liu Z, Lee S Y and Lee E C 2014 *Appl. Phys. Lett.* **105** 223306
[107] Aoki Y 2017 *Org. Electron.* **48** 194
[108] Zhang Y, Wang N, Wang Y, Zhang J, Liu J and Wang L 2021 *iScience* **24** 103104
[109] Kim T, Younts R, Lee W, Lee S, Gundogdu K and Kim B J 2017 *J. Mater. Chem.* A **5** 22170
[110] Chen N, Kovacik P, Howden R M, Wang X, Lee S and Gleason K K 2015 *Adv. Energy Mater.* **5** 1401442
[111] Vandenbergh J *et al* 2011 *Macromolecules* **44** 8470